HHS Public Access

Author manuscript

Nature. Author manuscript; available in PMC 2024 December 12.

Published in final edited form as:

Nature. 2024 June ; 630(8018): 976–983. doi:10.1038/s41586-024-07537-3.

CTLA-4 expressing ILC3s restrain interleukin-23 mediated inflammation

Anees Ahmed[1,2,3], **Ann M Joseph**[1,2,3], **Jordan Zhou**[1,2,3], **Veronika Horn**[1,2,3], **Jazib Uddin**[1,2,3], **Mengze Lyu**[1,2,3], **Jeremy Goc**[1,2,3], **JRI Live Cell Bank**[3], **Robbyn E. Sockolow**[4], **James B. Wing**[5,6,7], **Eric Vivier**[8], **Shimon Sakaguchi**[5,9], **Gregory F. Sonnenberg**[1,2,3,*]

[1]Joan and Sanford I. Weill Department of Medicine, Division of Gastroenterology & Hepatology, Weill Cornell Medicine, Cornell University, New York, NY, USA

[2]Department of Microbiology & Immunology, Weill Cornell Medicine, Cornell University, New York, NY, USA

[3]Jill Roberts Institute for Research in Inflammatory Bowel Disease, Weill Cornell Medicine, Cornell University, New York, NY, USA

[4]Department of Pediatrics, Division of Gastroenterology, Hepatology, & Nutrition, Weill Cornell Medicine, Cornell University, New York, NY, USA

[5]Laboratory of Experimental Immunology, World Premier International Immunology Frontier Research Center, Osaka University, Suita 565-0871, Japan

[6]Laboratory of Human Single Cell Immunology, WPI IFReC, Osaka University, Suita 565-0871, Japan

[7]Human Single Cell Immunology Team, Center for Infectious Disease Education and Research, Osaka University, Suita, Japan

[8]Innate Pharma Research Laboratories, Innate Pharma, Marseille, France; Aix Marseille University, CNRS, INSERM, CIML, Marseille, France; APHM, Hôpital de la Timone, Marseille-Immunopôle, Marseille, France; Paris Saclay Cancer Cluster, Villejuif, France

[9]Department of Experimental Pathology, Institute for Frontier Medical Sciences, Kyoto University, Kyoto 606-8507, Japan

[*]Correspondence and requests for materials should be addressed to gfsonnenberg@med.cornell.edu.

Author contributions

A.A. and G.F.S. conceived the project. A.A. performed most experiments and analyzed the data. A.M.J., J.Z., V.H., J.U., M.L and J.G. helped with experiments and data analyses. JRI Live Cell Bank and R.E.S. contributed to clinical sample acquisition, annotation, processing, and evaluation. J.B.W., E.V. and S.S. provided essential mouse models, scientific advice, and expertise. A.A. and G.F.S. wrote the manuscript, with input from all the authors.

JRI Live Cell Bank consortium members

David Artis[3], Randy Longman[3], Gregory F. Sonnenberg[3], Ellen Scherl[3], Robbyn Sockolow[3], Dana Lukin[3], Vinita Jacob[3], Laura Sahyoun[3], Michael Mintz[3], Lasha Gogokhia[3], Thomas Ciecierega[3], Aliza Solomon[3], Arielle Bergman[3], Kimberley Chein[3], Elliott Gordon[3], Michelle Ramos[3], Victoria Ribeiro de Godoy[3], Adriana Brcic-Susak[3], Seun Oguntunmibi[3], Dario Garone[3], Caitlin Mason[3].

[3]Jill Roberts Institute for Research in Inflammatory Bowel Disease, Weill Cornell Medicine, Cornell University, New York, NY, USA.

Reporting summary

Further information on research design is available in the Nature Portfolio Reporting Summary linked to this article.

The authors declare no competing interests.

Abstract

Interleukin (IL-)23 is a major mediator and therapeutic target in chronic inflammatory diseases, that also elicits tissue-protection in the intestine at homeostasis or following acute infection[1–4]. However, the mechanisms shaping these beneficial versus pathologic outcomes remain poorly understood. To address this gap in knowledge, we performed single cell RNA-sequencing on all IL-23 receptor expressing cells in the intestine and their acute response to IL-23, revealing a dominance of T cells and group 3 innate lymphoid cells (ILC3s). Unexpectedly, we identified potent upregulation of the immunoregulatory checkpoint molecule, cytotoxic T-lymphocyte-associated antigen-4 (CTLA-4), on ILC3s. This pathway was activated by gut microbes and IL-23 in a FOXO1- and STAT3-dependent manner. Mice lacking CTLA-4 on ILC3s exhibit reduced regulatory T cells, elevated inflammatory T cells, and more severe intestinal inflammation. IL-23 induction of CTLA-4$^+$ ILC3s was necessary and sufficient to reduce co-stimulatory molecules and increase PD-L1 bioavailability on intestinal myeloid cells. Finally, human ILC3s upregulate CTLA-4 in response to IL-23 or gut inflammation and correlate with immune regulation in inflammatory bowel disease (IBD). These results reveal ILC3-intrinsic CTLA-4 as an essential checkpoint that restrains the pathologic outcomes of IL-23, suggesting that disruption of these lymphocytes, which occurs in IBD[5–7], contributes to chronic inflammation.

IL-23 is a heterodimeric cytokine belonging to the IL-12 family, encompassing a shared IL-12p40 subunit and specific IL-23p19 subunit[1,8,9]. Basic mouse models, genetic studies in patients, and clinical trials identified that IL-23 is a major mediator of autoimmune and chronic inflammatory disorders, including inflammatory bowel disease (IBD)[9], psoriasis[10], rheumatoid arthritis[11], and multiple sclerosis[12]. For example, genome-wide association studies identified single-nucleotide polymorphisms in IL-23 receptor (IL-23R) loci that strongly associate with disease pathogenesis[13,14], and blocking IL-23 provides therapeutic benefit in a subset of patients[15–17]. However, IL-23 exhibits numerous beneficial, anti-microbial, and tissue protective functions. This is particularly evident in the intestine, where IL-23 is produced in response to microbiota colonization, and blockade of IL-23 alters microbiota composition[18], increases susceptibility to enteric infections[19–21], or in some cases exacerbates gut inflammation[22,23]. Further, humans with loss-of-function mutations in *IL23R* are more susceptible to various bacterial and fungal infections at mucosal surfaces[24]. This creates a paradigm that IL-23 mediates both tissue protective and pathologic responses, particularly in the intestine, but the cellular and molecular mechanisms controlling these disparate outcomes remains unclear.

Mapping IL-23 responses in the small intestine

To comprehensively define the IL-23 pathway, we performed single-cell RNA sequencing (scRNA-seq) of all IL-23R$^+$ cells in the small intestine of healthy IL-23R-eGFP reporter mice, as well as the acute response of these populations to *ex vivo* stimulation with IL-23 (Extended Data Fig. 1a). A total of 10,325 unstimulated cells and 8,897 cells with IL-23 stimulation were included in our analyses. Six distinct clusters of IL-23R$^+$ cells were identified, and each annotated based on select marker genes and visualized by uniform manifold approximation and projection (UMAP). These cell types include well-described subsets of group 3 innate lymphoid cells (ILC3s), γδ T cells, T_H17 cells, and a minor

proliferative cluster with high *Mki67* expression (Fig. 1a,b and Extended Data Fig. 1b,c). The IL-23R$^+$ ILC3 subsets encompass NKp46$^+$ or T-bet$^+$ ILC3s, CCR6$^+$ lymphoid tissue-inducer (LTi)-like ILC3s, and CCR6$^-$ NKp46$^-$ double-negative (DN) ILC3s. We validated these results by unbiased flow cytometry using IL-23R-eGFP mice and quantitatively determined selective expression of IL-23R in these cells, as well as in the large intestine of naïve mice or following *Citrobacter* rodentium infection (Extended data Fig. 2a–c). Upon acute IL-23 stimulation, we observed robust transcriptional changes predominantly among the ILC3 subsets and modest transcriptional changes in T cells (Fig. 1c and Extended Data Fig. 3a,b). Several expected transcriptional changes were observed, including engagement of IL-17 and IL-22, however, we also observed potent upregulation of the immunoregulatory checkpoint molecule, CTLA-4, among the NKp46$^+$ and DN ILC3 subsets, as well as in γδ T cells to a lesser extent (Fig. 1c and Extended Data Fig. 3a,b). Given this unexpected finding, we next profiled cellular sources of CTLA-4 protein by unbiased flow cytometry in the healthy C57BL/6 mouse small intestine. Regulatory T cells (Tregs) are the dominant cell type expressing CTLA-4, however, we also found a sizable proportion of CTLA-4$^+$ cells lack lineage markers and are ILC3s (Fig. 1d,e). NKp46$^+$ ILC3s express the most CTLA-4 relative to other innate lymphocytes (Extended Data Fig. 4a,b). A majority of the CTLA-4$^+$ ILC3s co-express T-bet, and consistent with prior reports of IL-23-dependent hyperactivation in the absence of adaptive immunity[25,26], ILC3s express significantly more CTLA-4 in the small intestine of *Rag1*$^{-/-}$ mice (Fig. 1f). In this setting, ILC3s are the dominant CTLA-4$^+$ cell type in the small intestine (Fig. 1g and Extended Data Fig. 4c). These data provide a comprehensive single-cell atlas of all IL-23R$^+$ immune cells in the healthy mammalian intestine and following acute IL-23 activation, which revealed a previously unappreciated upregulation of the immunoregulatory checkpoint molecule CTLA-4 on ILC3s.

A microbe-IL-23 axis drives CTLA-4$^+$ ILC3s

The intestinal microbiota is required for the proper development and function of ILC3s[27,28]. To investigate whether intestinal microbiota is required for ILC3-intrinsic CTLA-4, we profiled the large and small intestine of mice that are specific-pathogen-free (SPF), germ-free, or exposed to broad-spectrum antibiotics. Notably, both germ-free *Rag1*$^{-/-}$ mice or specific pathogen free *Rag1*$^{-/-}$ mice that were exposed to broad-spectrum antibiotics displayed a significant reduction of CTLA-4 protein in ILC3s relative to controls (Fig. 2a,b). Limited staining of microbiota-dependent CTLA-4 was observed in ILC1s and NK cells (Extended Data Fig. 5a,b). To determine the signals that directly promote CTLA-4 in ILC3s, we stimulated intestinal cells with canonical activators IFN-γ, IL-1β, IL-2, IL-6, IL-7, IL-12, IL-15 or IL-23[27,28]. Among these, IL-23 robustly and selectively induced CTLA-4 protein in ILC3s, while IL-12 induced CTLA-4 in ILC1s (Fig. 2c,d and Extended Data Fig. 5c). IL-23 potently upregulated CTLA-4 in ILC3s, with modest changes in γδ T cells, and this was not sufficient to modulate CTLA-4 in Tregs or T_H17 cells (Fig. 2e and Extended Data Fig. 5c). Further, the frequency of CTLA-4$^+$ ILC3s was significantly reduced upon *in vivo* blockade of IL-23 using a monoclonal antibody (Fig. 2f). FOXO1 and STAT3 are two downstream pathways engaged by IL-23R signaling and linked to CTLA-4 expression in Tregs[29,30]. We found that inhibition of either FOXO1 or STAT3 activation

significantly limited IL-23-mediated induction of CTLA-4 in ILC3s (Fig. 2g). We next investigated whether diverse microbial encounters or chronic inflammatory environments regulate ILC3-intrinsic CTLA-4. Notably, overexpression of IL-23 in mice with a minicircle vector resulted in significantly increased ILC3-intrinsic CTLA-4 in the large intestine (Fig. 2h). ILC3-specific CTLA-4 was also upregulated in the large intestine following exposure of SPF mice to diverse microbes by co-housing with pet store mice, in the context of IL-10-deficiency and spontaneous gut inflammation, or upon infection with *C. rodentium* in an IL-23-dependent manner (Fig. 2i–k). These data demonstrate that microbiota colonization of the intestine and associated induction of IL-23 support the presence of CTLA-4$^+$ ILC3s at homeostasis in a FOXO1 and STAT3-dependent manner, and that this pathway is further engaged in the context of diverse microbial exposure, enteric infection, or chronic inflammation.

CTLA-4$^+$ ILC3s restrain gut inflammation

To explore the functional significance of this pathway, we generated mice with a deletion of CTLA-4 in ILC3s by crossing NKp46-cre mice with CTLA-4 floxed mice. This approach was selected since CTLA-4 is dominantly expressed on the NKp46$^+$ ILC3 subset, and with unbiased gating on all NKp46$^+$ cells, we observe that ILC3s are the major subtype that is CTLA-4$^+$ at homeostasis and following *C. rodentium* infection (Extended Data Fig. 6a,b). The resulting *Ncr1^{cre} Ctla4$^{f/f}$* mice demonstrated a deletion of CTLA-4 on T-bet$^+$ ILC3s, without impacting CTLA-4 on T cells (Fig. 3a). These mice exhibit comparable frequencies, subset distribution, and cytokine production among various immune cells in the large intestine at homeostasis (Extended data Fig. 6c–g). We next investigated the role of CTLA-4$^+$ ILC3s using the enteric pathogen *C. rodentium*, which induces potent upregulation of IL-23 to drive optimal immunity[19–21]. In this context, there was no significant difference of pathogen burden, or in the frequencies of ILC3s and IL-22 production in the large intestine of *Ncr1^{cre} Ctla4$^{f/f}$* mice relative to littermate controls (Fig. 3b–d). IL-23 is also linked to reducing the stability and functionality of Treg responses[23,31,32]. Therefore, despite this intact immunity to *C. rodentium*, we profiled the adaptive immune response during infection and found a significant reduction in the frequency of Tregs and significant elevation of pro-inflammatory T cells that co-produce IFNγ and IL-17A in the colon of mice lacking CTLA-4$^+$ ILC3s relative to littermate controls (Fig. 3e,f). Consistent with this imbalance in effector and regulatory T cell responses, *Ncr1^{cre} Ctla4$^{f/f}$* mice exhibited significantly elevated colonic neutrophils, shorter colon length, and increased histologic evidence of intestinal inflammation (Fig. 3g–i). NK cells and ILC1s had minimal levels of CTLA-4 in the healthy gut that were unchanged during *C. rodentium* infection (Extended data Fig. 7a). Depletion of these cells, but not ILC3, with an anti-NK1.1 antibody during *C. rodentium* infection did not alter the inflammatory outcomes of mice (Extended data Fig. 7b–f). Loss of one copy of NKp46 or *Ncr1* also did not impact inflammation in the large intestine following *C. rodentium* infection (Extended data Fig. 8a–d). These results collectively indicate that CTLA-4 is upregulated on ILC3s in response to an enteric pathogen and IL-23 to subsequently restrain inflammatory T cell responses and promote immune regulation.

To validate this finding, we also generated *Rag1*$^{-/-}$ RORγt^{cre} *Ctla4*$^{f/f}$ mice and examined the functional significance of ILC3-specific CTLA-4 in models of intestinal inflammation induced by anti-CD40 agonistic antibody[33] or naïve T cell transfer[34]. Interestingly, despite robust CTLA-4 deletion in ILC3s, the agonistic anti-CD40 model in *Rag1*$^{-/-}$ RORγt^{cre} *Ctla4*$^{f/f}$ mice revealed comparable ILC3 responses as well as parameters of intestinal inflammation including leukocyte infiltration and colonic shortening relative to littermate controls (Extended data Fig. 8e–i). This demonstrates that ILC3-specific CTLA-4 is dispensable when T cells are absent and is consistent with the intact innate immunity observed in this model and the *C. rodentium* infection model. In contrast, during the naïve T cell transfer model, which is driven by adaptive immunity and dependent upon IL-23[34], we observed mice lacking ILC3-specific CTLA-4 exhibit a significantly greater weight loss, frequency of T_H17 cells, production of TNF and IFNγ from colonic T cells, colonic neutrophil infiltration, shorter colon length, and increased histologic evidence of intestinal inflammation relative to littermate controls (Fig. 3j–o). These data demonstrate that ILC3-specific CTLA-4 is necessary to restrain inflammatory T cell responses and promote immune regulation in mouse models of IL-23-driven colitis.

CTLA-4$^+$ ILC3s shape gut co-stimulation

CTLA-4, particularly on Tregs, mediates critical immunosuppressive functions[35,36]. This occurs in part through CTLA-4 dependent trogocytosis of CD80 and CD86 on myeloid cells, restricting the activation of effector T cells in autoimmunity and chronic inflammation[37,38]. Therefore, we next examined whether CTLA-4$^+$ ILC3s modulate co-stimulatory molecules on intestinal myeloid cells and in response to IL-23. We found that IL-23 primarily drives upregulation of the membrane-bound compared to the soluble form of CTLA-4 on ILC3s (Fig. 4a). We also profiled co-stimulatory molecules on large intestine myeloid cells following *C. rodentium* infection and found that mice lacking CTLA-4$^+$ ILC3s exhibit significantly increased levels of CD80 and CD86 on myeloid cells relative to littermate controls (Fig. 4b,c). Recent seminal studies indicate that CD80 interacts with PD-L1 in a cis-manner on myeloid cells, which prevents PD-L1 on myeloid cells from interacting with PD-1 on other cell types[39,40]. It was recently demonstrated that CTLA-4$^+$ Tregs decrease this cis-interaction through the trogocytosis of CD80 to increase the bioavailability of free PD-L1 on myeloid cells[39], while other prior studies indicate that PD-L1 signals from myeloid cells support the generation or maintenance of PD-1$^+$ Tregs[41,42]. Consistent with this, we found that with the increase in co-stimulatory molecules, there was significant reduction in the bioavailability of free PD-L1 on myeloid cells from mice lacking CTLA-4$^+$ ILC3s during *C. rodentium* infection (Fig. 4d). Similarly, *Rag1*$^{-/-}$ RORγt^{cre} *Ctla4*$^{f/f}$ mice lacking CTLA-4$^+$ ILC3s and receiving a naïve T cell transfer exhibit significantly increased levels of CD80 and CD86 with a significant reduction in the bioavailability of free PD-L1 on myeloid cells from the large intestine relative to littermate controls (Fig. 4e–g). We next asked whether CTLA-4 from ILC3s is sufficient to impart these outcomes using an *ex vivo* co-culture system. Notably, we found that co-culture of ILC3s and myeloid cells from the large intestine following exposure to heat killed *C. rodentium*, or in the presence of recombinant IL-23, resulted in a significant reduction of CD80 and CD86 on myeloid cells (Fig. 4h,i and Extended data Fig. 9a,b). In both settings, blockade of either IL-23 or

CTLA-4 reversed this downregulation of CD80 and CD86 on intestinal myeloid cells (Fig. 4h,i and Extended data Fig. 9a,b). ILC3 co-culture also resulted in significantly increased bioavailability of PD-L1 on myeloid cells in both a CTLA-4- and IL-23-dependent manner (Fig. 4j and Extended data Fig. 9c). These data demonstrate that IL-23 drives upregulation of CTLA-4 on ILC3s that is necessary and sufficient to reduce co-stimulatory molecules on gut myeloid cells and increase bioavailability of the key immune-regulatory molecule PD-L1.

CTLA-4$^+$ ILC3s are altered in IBD

We next explored for clinical relevance and whether this pathway is functional in humans. We found in an *ex vivo* culture that IL-23 was sufficient to significantly upregulate CTLA-4 in human ILC3s derived from tonsils (Fig. 5a). To explore this pathway in a disease setting, we performed bulk RNA sequencing on ILC3s sorted from the inflamed intestine or matched adjacent non-inflamed intestine that were resected from IBD patients, encompassing both Crohn's disease and ulcerative colitis (Supplementary Table 1). We identified 254 genes which were upregulated and 79 genes which were downregulated in ILC3s from inflamed tissue relative to adjacent non-inflamed intestine, and interestingly, among these differentially upregulated genes, a notable significant increase in *CTLA4* was observed in ILC3s (Fig. 5b). We validated this by performing profiling of intestinal biopsies from IBD patients versus age- and gender-matched controls (Supplementary Table 2). We observed a significantly increased frequency of CTLA-4$^+$ ILC3s in patients with Crohn's disease relative to healthy controls (Fig. 5c and Extended Data Fig. 9d). Notably, we identified a significant positive correlation between the frequencies CTLA-4$^+$ ILC3s and free PD-L1$^+$ intestinal myeloid cells within the same biopsy of IBD patients (Fig. 5d). Further, the abundance of free PD-L1 on myeloid cells exhibited a significant positive correlation with Treg frequencies (Fig. 5e). These data sets reveal that human ILC3s upregulate CTLA-4 in response to IL-23 or in the inflamed intestine, and that this pathway correlates with immune regulatory checkpoints during disease. However, as previously reported[5–7], we also observed a significantly reduced frequency of overall ILC3s in intestinal biopsies from patients with Crohn's disease relative to those from healthy controls (Fig. 5f), indicating that this pathway can become compromised in IBD patients.

Discussion

Here we identify ILC3s as a critical link between potent IL-23 driven inflammatory and immunoregulatory checkpoints in the intestine. This provokes a model whereby microbial exposure induces IL-23 to subsequently upregulate CTLA-4 on ILC3s, which then supports immune regulation by reducing co-stimulatory molecules, CD80 and CD86, and increasing bioavailability of PD-L1 on myeloid cells (Extended data Fig. 10). Impairment of this pathway manifests in a substantial imbalance of effector and regulatory T cell responses and enhanced intestinal inflammation. This is a key conceptual advance in our understanding of how IL-23 functions at homeostasis and in a tissue protective manner following exposure to diverse microbes. It is entirely distinct from our prior studies detailing how IL-2-producing ILC3s support Tregs in the small intestine[7], or how antigen presenting ILC3s instruct differentiation of microbiota-specific Tregs[43], both of which occur at steady state and are independent of IL-23. Further, it indicates that ILC3-specific CTLA-4 counteracts

the appreciated inhibitory roles of IL-23 on Tregs[23,31,32], likely through PD-L1[41]. This is particularly important in the gastrointestinal tract, which is regularly colonized with beneficial microbiota, opportunistic microbes, or enteric pathogens that induce robust and local IL-23 production. Therefore, these tissue-resident ILC3 responses critically balance this pro-inflammatory cytokine to maintain gut homeostasis. It remains possible that CTLA-4 is functionally important by other innate or innate-like lymphocytes following exposure to different signaling cues. ILC3s are known to be depleted from the gut in the setting of chronic IL-23 exposure in mouse models[44,45], or in chronic diseases such as IBD[5–7,43,46], colorectal cancer[47], and various infections[48]. Therefore, although we find that this pathway is functional in humans, disrupted engagement of IL-23-dependent CTLA-4$^+$ ILC3s could shift the balance from immune regulation to inflammation, which may represent a key transition that supports the pathogenesis of chronic inflammatory diseases. Finally, this study also informs the use of CTLA-4 blockade in the context of cancer immunotherapy, which can provide a substantial therapeutic benefit but often manifests in checkpoint-induced colitis as an immune related adverse event[49,50]. Advances to support CTLA-4$^+$ ILC3s and engagement of the PD-L1 pathway represent an opportunity to counteract aberrant IL-23-driven chronic inflammation.

Materials and methods

Data reporting.

No statistical methods were used to predetermine sample size. The animal experiments were not randomized because littermate group allocation was based on animal genotype; thus, investigators were not blinded to allocation during experiments and data assessment. All experiments were successfully replicated and were independently performed at least two times unless otherwise mentioned.

Mice.

C57BL/6 mice, *Rag1*$^{-/-}$ mice[51], *Il10*$^{-/-}$ mice[52], and IL-23R-eGFP KI mice[53] on a C57BL/6 background were purchased from the Jackson Laboratory and used at 6–12 weeks of age. RORγt^{cre} mice[54] on a C57BL/6 background were provided by Dr. Gerard Eberl (Institut Pasteur). C57BL/6 *Ncr1*^{cre} mice[55] were provided by Dr. Eric Vivier and *Ctla4*-floxed mice[35] were provided by Dr. Shimon Sakaguchi. Germ free mice were maintained at the gnotobiotic facility at Weill Cornell Medicine. Both female and male mice were used in this study. All transgenic mice were bred and maintained in specific pathogen free facilities with a 12-hour light–dark cycle, an average ambient temperature of 21°C and an average humidity of 48% at Weill Cornell Medicine. Littermates were used as controls, and sex- and age-matched mice were used in all experiments. In any of these experiments sex was not found to influence the outcome of the results. No mice were excluded from the analysis unless clearly indicated. All experiments were approved and performed according to the Institutional Animal Care and Use Committee guidelines at Weill Cornell Medicine.

Isolation of lamina propria immune cells from the intestine of mice.

Whole intestines were aseptically removed from the mice and cleaned by removing the fat tissues. For small intestine, Peyer's patches were carefully removed. Afterwards, intestines

were opened longitudinally, extensively cleaned with cold Dulbecco's PBS (Corning) and cut approximately into 0.5 cm sections. To dissociate epithelial cells, cut tissues were incubated in Hanks' balanced salt solution) containing 5 mM EDTA (Thermo Fisher Scientific), 1 mM dithiothreitol (Sigma-Aldrich) and 2% fetal bovine serum twice at 37 °C for 20 minutes. After incubation, the tissues were vortexed, transferred to digestion buffer containing collagenase III (1 mg mL^{-1}; Worthington), dispase (0.4 U mL^{-1}; Thermo Fisher Scientific), DNase I (20 μg mL^{-1} ;Sigma-Aldrich) and 10% FBS in RPMI 1640 (Corning), and incubated in a shaker at 200 rpm for 1 hour at 37°C. Leukocytes were enriched by 40/80% density gradient Percoll centrifugation (GE Healthcare).

Flow cytometry and cell sorting.

Single-cell suspensions were first blocked with anti-CD16/32 antibody (BD Biosciences, 2.4G2) and then incubated with conjugated antibodies in phosphate-buffered saline (PBS) containing 1% FBS and 0.25 mM EDTA on ice. Dead cells were excluded by Fixable Aqua Dead Cell Stain (Thermo Fisher Scientific). The flow cytometry antibodies were purchased from Thermo Fisher Scientific, Biolegend or BD Bio-sciences. Antibodies targeting TCRβ (H57-597), B220 (RA3-6B2), CCR6 (29-2L17), CD3ε (145-2C11), CD4 (RM4-5), CD5 (53-7.3), CD8α (53-6.7), CD11b (M1/70), CD11c (N418), Ly6G (1AB-Ly6G), CD19 (eBio1D3), TCRγδ (GL3), CD45 (30-F11), CD64 (X54-5/7.1), CD90.2 (30-H12), CD127 (A7R34), F4/80 (BM8), MHCII (M5/114.15.2), NK1.1 (PK136), NKp46 (29A1.4), CD117 (ACK2), CD25 (PC61.5), CD80 (16-10A1), CD86 (GL-1), PD-L1 total (1-111A), PD-L1 free (10F. 9G2) and KLRG1 (2F1/KLRG1) were used for surface staining. CTLA-4 (UC10-4B9), FOXP3 (FJK-16S), GATA3 (L50- 823), EOMES (Dan11mag), IL-17A (eBio 17B7), IL-22 (IL22JOP), IFNγ (XMG1.2), Ki67 (SolA15), RORγ (B2D), anti-rabbit IgG (Poly 4064), rat IgG1 isotype control (R3-34) and T-bet (eBio4B10) were used for intracellular staining. Lineage markers for mouse are: CD3ε, CD5, CD8α, NK1.1, TCRγδ, Ly6G, CD11b, CD11c, B220, F4/80. All mouse antibodies were used at 1:200 dilution, except for CCR6, NKp46 and CTLA-4, which were used at 1:100 dilution. For PD-L1 staining, mouse myeloid cells were first stained with 1-111A anti–PD-L1 mAb, to detect total (CD80 bound and free) PD-L1 molecules and then incubated with 10F.9G2 PD-L1 mAb, which competes with CD80 for binding and stain-free PD-L1. The following antibodies were used for cell-surface staining of human samples: CD3 (UCHT1), CD14 (M5E2), CD19 (HIB19), CD34 (581), CD4 (SK3), CD45 (HI30), CD94 (DX22), CD117 (104D2), CD123 (6H6), CD127 (A019D5), FcεR1 (AER-37(CRA1), PD-L1 (29E.2A3), CD11c (S-HCL-3), MHCII (L243), CD86 (IT2.2), CD80 (B7-1) and NKp44 (44.189). For Free PD-L1 staining, cells were incubated with biotinylated recombinant human PD-1 (CD279)-Fc chimera (Biolegend) followed by PE-Cy5-streptavidin. The following antibodies were used for intracellular staining of human samples: FOXP3 (PCH101), CTLA-4 (14D3), RORγ (Q21-559). All human antibodies were used at 1:100 dilution, except for CD45, and RORγ which were used at 1:50 dilution. Human ILC3s for analysis were gated as $CD45^+$ $CD3^-$ $CD11c^-$ $CD14^-$ $CD19^-$ $CD34^-$ $CD94^-$ $CD123^-$ $FcεR1^-$ $CD127^+$ $RORγ^+$. Human myeloid cells were gated as $CD45^+$ $CD3^-$ $CD4^-$ $CD11c^+$ $MHCII^+$. For transcription factors, cells were first stained for surface markers, followed by fixation and permeabilization according to the manufacturer's protocol (FOXP3 staining buffer set from Thermo Fisher Scientific, 00-5123-43). For cytokines, cells were stimulated in RPMI

1640 with 10% FBS, phorbol 12-myristate 13-acetate (PMA) 50 ng mL^{-1} (Sigma-Aldrich), ionomycin 750 ng mL^{-1} (Sigma-Aldrich) and brefeldin A 10 μg mL^{-1} (Sigma-Aldrich) for 4 hours. All flow cytometry experiments were performed on a Fortessa flow cytometer with FACS Diva software (BD Biosciences) and analyzed by FlowJo v.10 software. A FACSAria II cell sorter (BD Biosciences) was used for cell sorting.

Ex vivo stimulation.

Sort-purified mouse ILC3s (live, $CD45^+$ Lin^- $CD90^+$ $CD127^+$ $KLRG1^-$ $CD45^{dim}$) were cultured in RPMI with high glucose, supplemented with 10% FBS, 10 mM HEPES, 1 mM sodium pyruvate, non-essential amino acids, 80 μM 2-mercaptoethanol, 2 mM glutamine, 100 U/mL penicillin, 100 μg/mL streptomycin (all from Gibco) and Brefeldin A at 37 °C for 4 hours in the presence of recombinant mouse IFN-γ (20 ng/mL, Biolegend), IL-1β (20 ng/mL, Thermo Fisher Scientific), IL-2 (20 ng/mL, Biolegend), IL-6 (20 ng/mL, Thermo Fisher Scientific), IL-7 (20 ng/mL, Biolegend), IL-12 (20 ng/mL, Thermo Fisher Scientific), IL-15 (20 ng/mL, Biolegend), or IL-23 (20 ng/mL, Biolegend) or in presence or absence of Foxo1 inhibitor (AS1842856, 100 nM) or STAT3 inhibitor (VI-S3I-201, 25 μM). The cells were further stained and analyzed by flow cytometry. Similarly, immune cells from human tonsil were cultured with recombinant human IL-6 (20 ng/mL, Biolegend), recombinant human IL-2 (20 ng/mL, Biolegend) and recombinant human IL-21 (20 ng/mL, R&D) in presence or absence recombinant human IL-23 (50 ng/mL, Biolegend) with Brefeldin A at 37°C for 6 hours. The cells were further stained and analyzed by flow cytometry.

In vivo administration of antibodies and antibiotics.

Anti-IL-23p19 monoclonal antibodies (G23-8, BioXCell) were administered intraperitoneally at a dose of 300 μg per mouse every alternate day starting on day 0 and ending on day 5. Anti-NK1.1 monoclonal antibody (PK136, BioXCell) was administered intraperitoneally every 3 days at a dose of 300 μg per mouse starting on day 0 and ending on day 14. A cocktail of antibiotics (0.25 mg/mL of vancomycin, 0.5 mg/mL of ampicillin, neomycin, gentamicin and metronidazole, and 4 mg/mL sucralose) was continuously administered via drinking water for two weeks. Mice were regularly monitored for weight change.

Administration of minicircle vectors.

IL-23 and sham minicircle were purchased from System Biosciences, Inc. Hydrodynamic injection of 3-6 μg DNA will be carried out in sterile Ringer's solution equivalent to 10% mouse body weight and injected *i.v.* over 5-7 seconds.

C. rodentium infection.

C. rodentium was cultured in LB broth overnight at 37°C with constant shaking and mice were orally gavage with 10^9 CFUs of bacteria. Fecal pellets were collected at day 5 or 10 post infection and *C. rodentium* CFUs were enumerated by plating on MacConkey agar. Mice were euthanized at 14 days post infection for analysis. The colon length was measured, and distal colon was used for histological analysis.

Adoptive transfer of naïve CD4$^+$ T cells.

Naive CD4$^+$ T cells were isolated from the spleen and lymph nodes of C57BL/6 mice with a isolation kit following the manufacturer's instructions (Miltenyi Biotech). Recipient mice received 0.5 x 10^6 cells per mouse retro-orbitally. Mice were monitored for weight loss and analyzed at the indicated timepoint.

Co-culture of intestinal ILC3s and myeloid cells.

Myeloid cells (live, CD45$^+$ CD90.2$^-$ CD19$^-$ B220$^-$ CD11c$^+$ MHCII$^+$) and ILC3s (live, CD45$^+$ Lin$^-$ CD90$^+$ CD127$^+$ KLRG1$^-$ CD45^{dim}) were sort-purified from the large intestine of C57BL/6 mice and co-cultured, at the ratio 1:5 at 37°C with either recombinant IL-23 or heat killed *C. rodentium* and indicated blocking antibodies. After 6 or 24 hours, myeloid cells were first labeled with biotinylated 1-111A anti–PD-L1, then stained with streptavidin, 10F.9G2 anti–PD-L1, anti–CD11c, anti-MHCII, anti–CD80, anti-CD86 for flow cytometry analysis of CD80, CD86, and PD-L1.

Anti-CD40 mouse model colitis.

Indicated mice were treated intraperitoneally with 100 μg of anti-CD40 antibody (IgG2a, monoclonal Ab FGK45 from BioXCell) to induce innate colitis. Mice were analyzed and carefully monitored the following week for weight loss.

qPCR.

Sort-purified mouse ILC3s were stimulated with and without IL-23 for 2 hours and lysed using RLT plus lysis buffer (Qiagen). RNA was purified using RNeasy Plus Mini Kits (Qiagen) according to the manufacturer's instructions. First-strand cDNA was generated using Maxima First Strand cDNA synthesis kit according to the protocol provided by the manufacturer (Thermo Fisher Scientific, K1642). The Power SYBR Green PCR Master Mix (Thermo Fisher Scientific, 4367660) was used for qPCR with ABI7500 (Applied Biosystems). The primer sequences of soluble (s)CTLA-4 and membrane (m)CTLA-4 are as follows: Mouse sCTLA-4; forward: 5' - cgcagatttatgtcattgctaaag - 3'; reverse: 5' - aaacggcctttcagttgatg - 3'. Mouse mCTLA-4; forward: 5' - ggcaacgggacgcaga - 3'; reverse: 5'- cccaagctaactgcgacaagg - 3'. Gene expression was normalized to the internal controls *Hprt* for mouse samples.

scRNA sequencing.

For scRNA-seq, IL-23R$^+$ immune cells were sorted from small intestine of IL-23R-eGFP mice and stimulated with 30 ng/mL of recombinant mouse IL-23 for 2 hours. Cells were pooled from three mice. scRNA-seq libraries were generated using the 10X Genomics Chromium system with 3' version 3 chemistry. Libraries were sequenced on an Illumina NovaSeq instrument. Reads were processed by 10X Cell Ranger v.3.1.0 using the mm10 reference genome, resulting in a filtered HDF5 file. scRNA-seq data were further processed and analyzed using R v.4.1.2 and the Seurat package v.4.3.0 (ref.[56]). Specifically, the Cell Ranger output was imported using the Read10X_h5 function. Seurat objects were created using only genes that appeared in at least three cells. Cells were further filtered to exclude those with fewer than 1000 genes detected, more than 5,000 genes detected or more than

10% mitochondrial reads. Read counts were then normalized using the NormalizeData function. The graph representing cells with similar expression patterns was generated with the FindNeighbors function using the 20 largest principal components. A total of 10325 unstimulated cells and 8897 cells with IL-23 stimulation were included in our analyses. Cell clusters were generated using the Louvain algorithm implemented by the FindClusters function with the resolution parameter equal to 0.5. One cluster lacking *Il23r* expression was removed from the analysis and the remaining cells were re-clustered using a resolution of 0.6. Marker genes for each cluster were determined using the Wilcoxon test on the raw counts, implemented by the function FindAllMarkers, and including only positive marker genes with log fold changes greater than 0.25 and Bonferroni-corrected *P* values less than 0.01. Cluster names were determined by manual inspection of the lists of cluster marker genes. Dimensionality reduction by UMAP was performed using the RunUMAP function with the 20 largest principal components. All visualizations of scRNA-seq data were generated using the Seurat package as well as ggplot2 v.3.3.3.

Human sample collection.

Human tonsil and surgical resection samples from IBD patients were provided by the Cooperative Human Tissue Network (CHTN), which is funded by the National Cancer Institute. Other investigators may have received specimens from the same patients. Samples were received as entirely de-identified human specimens with diagnoses confirmed by medical records and trained pathologists. This protocol was reviewed by the Weill Cornell Medicine institutional review board and determined to meet the exemption category 4 of HHS 45 CFR 46.104(d). Additional oversight of the Cooperative Human Tissue Network is outlined at www.chtn.org. Intestinal biopsies from the colon of individuals with Crohn's disease and sex- and age-matched controls without IBD, were obtained following Institutional Review Board approved protocols from the JRI Live Cell Bank Consortium at Weill Cornell Medicine (protocol number 1503015958). Informed consent was obtained from all subjects. Biopsies were cryopreserved in 90% FBS and 10% DMSO for future side-by-side comparison.

Human tissue processing and isolation of ILC3s.

Human surgical intestinal samples were incubated with continuous shaking in PBS containing 5% FBS, 1 mM EDTA and 1 mM DTT for 30 minutes at 37 °C to remove the epithelial cells. After incubation, the tissues were vortexed, similarly transferred to digestion buffer containing 2 mg/mL Collagenase D (Sigma) and 0.1 μg/mL DNase I (Sigma) in RPMI 1640 (Corning) with 5% FBS for 1 hour. After digestion, the single cell suspension was passed through a 70 μM cell strainer to obtain the cells. Further, the cells were immediately cryopreserved for future use. For sorting human ILC3s, frozen samples were thawed, washed once in RPMI with 5% FBS, treated with Fc receptor block (BD Biosciences, 2.4G2) for 10 minutes, and surface stained. ILC3s were sorted as Live $CD45^+$ $Lineage^-$ (CD3e, CD34, CD19, CD94, CD14, CD123, FcεRIa, CD11c) $CD127^+$, $CRTH2^-$, $CD117^+$ cells. Tonsil samples were dissociated mechanically by a syringe plunger and cells were filtered through 70 mm cell strainer and cryopreserved in 90% FBS and 10% DMSO for a future side-by-side comparison. Following thawing, cells were used directly for staining. Intestinal biopsies were immediately cryopreserved in 90% FBS and 10% DMSO

for future side-by-side comparison. Following thawing, tissues were incubated in 0.5 mg/ml collagenase D and 20 mg/ml DNase I for 1 hour at 37°C with shaking. After digestion, remaining tissues were further dissociated mechanically by a syringe plugger. Cells were filtered through a 70 μM cell strainer and used directly for staining.

Bulk RNA sequencing.

ILC3s gated as Live CD45$^+$ Lineage$^-$ (CD3e, CD34, CD19, CD94, CD14, CD123, FcεRIa, CD11c) CD127$^+$, CRTH2$^-$, CD117$^+$ were sorted from the inflamed and matched adjacent non-inflamed intestine that was resected from IBD patients, encompassing both Crohn's disease and ulcerative colitis. These cells were used to prepare RNA sequencing libraries by the Epigenomics Core at Weill Cornell Medicine, using the Clontech SMARTer Ultra Low Input RNA Kit V4 (Clontech Laboratories). Sequencing was performed on an Illumina HiSeq 4000, yielding 50-bp single-end reads. Raw sequencing reads were demultiplexed with Illumina CASAVA (v.1.8.2). Adapters were trimmed from reads using FLEXBAR (v.2.4) and reads were aligned to the NCBI GRCh37/hg19 human genome using the STAR aligner (v.2.3.0) with default settings. Reads per gene were counted using Rsubread. Prior to differential expression analysis, genes were prefiltered, keeping only those genes with 50 or more counts in at least two samples. Differential expression analysis was performed using DESeq2 (version 1.20.0) using both site (inflamed/adjacent) and patient ID as factors in the design. A false discovery rate of 0.1 was taken to indicate significance. The volcano plot was generated using dplyr (v. 1.1.3), ggplot2 (v.3.4.3), and ggrepel (v. 0.9.3) in R (v 4.1.2).

Histological staining and blinded histopathologic scoring.

Large intestinal swiss rolls were fixed in 4% paraformaldehyde and embedded in paraffin. Five-micrometer sections were stained with H&E. Images were taken using a Nikon Eclipse Ti microscope and NIS-Elements 4.30.02 software (Nikon). Histological scoring of H&E-stained tissues was done following these parameters. Each mouse was scored in a blinded manner on a grade of 0–4 (0 = none; 4 = most severe) for the following four pathologic parameters for a maximum score of 16: (1) inflammatory cell infiltration; (2) goblet-cell depletion; (3) mucosa thickening/edema; and (4) destruction of crypt architecture.

Statistical analysis.

All statistical analyses were performed by Graph Pad Prism v.9 software. Mann–Whitney *U* test or one-way ANOVA with 95% confidence interval followed by Dunnett's multiple comparisons were used to determine the *P* values for the datasets. Correlative analyses were compared by nonparametric Spearman correlation. *P* values smaller than 0.05 were considered significant.

Extended Data

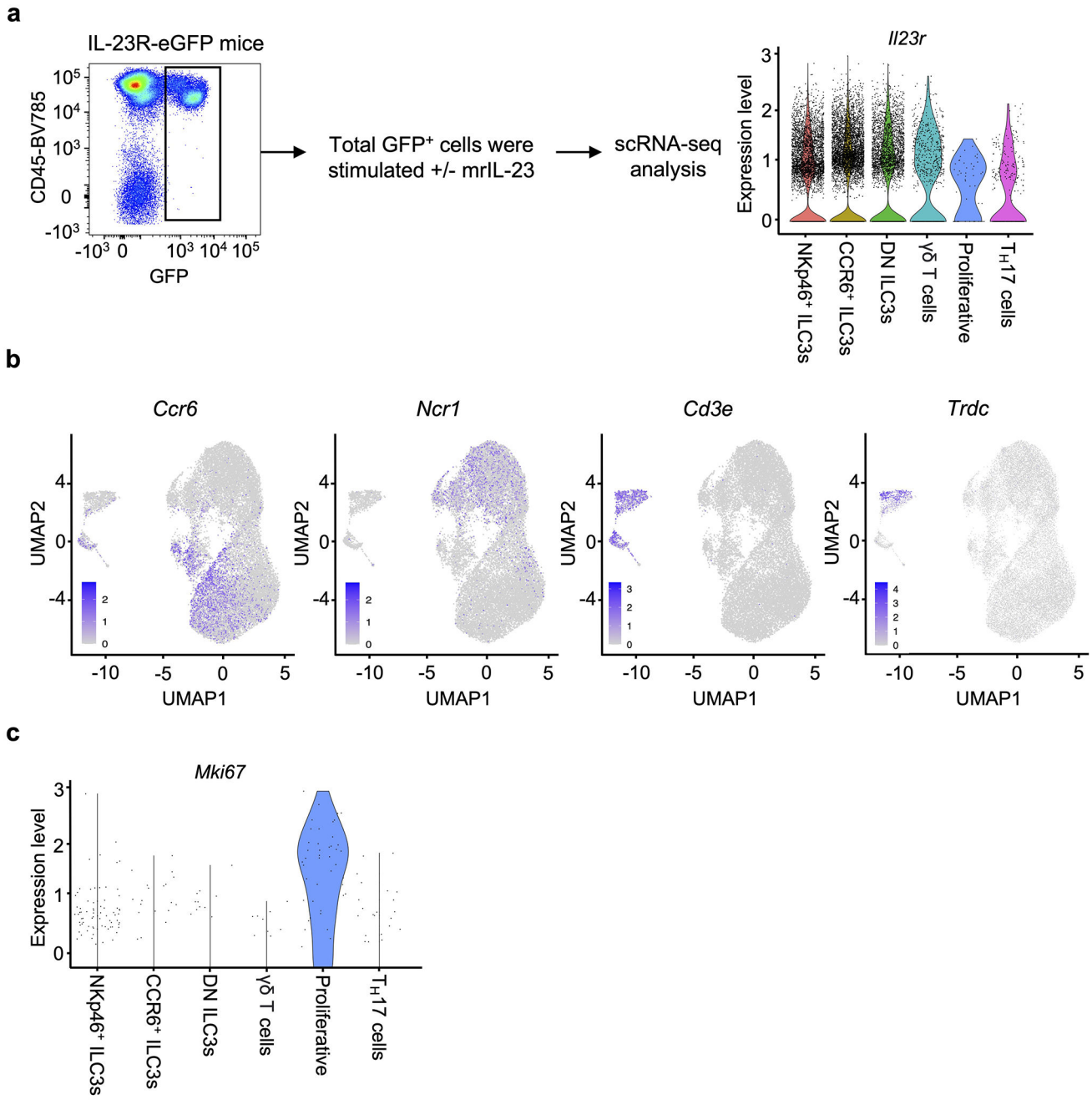

Extended Data Fig. 1 |. Single cell analysis of all IL-23R$^+$ cells in small intestine of healthy mice.
a, Gating strategy and experimental design to sort IL-23R$^+$ immune cells from small intestine lamina propria of IL-23R-eGFP mice for scRNA-seq. Violin plot confirming *Il23r* expression among all the identified IL-23R$^+$ cell clusters. **b,** Feature plots showing expression of indicated genes in different clusters. **c,** Violin plot showing *Mki67* expression among all identified IL-23R$^+$ cell clusters.

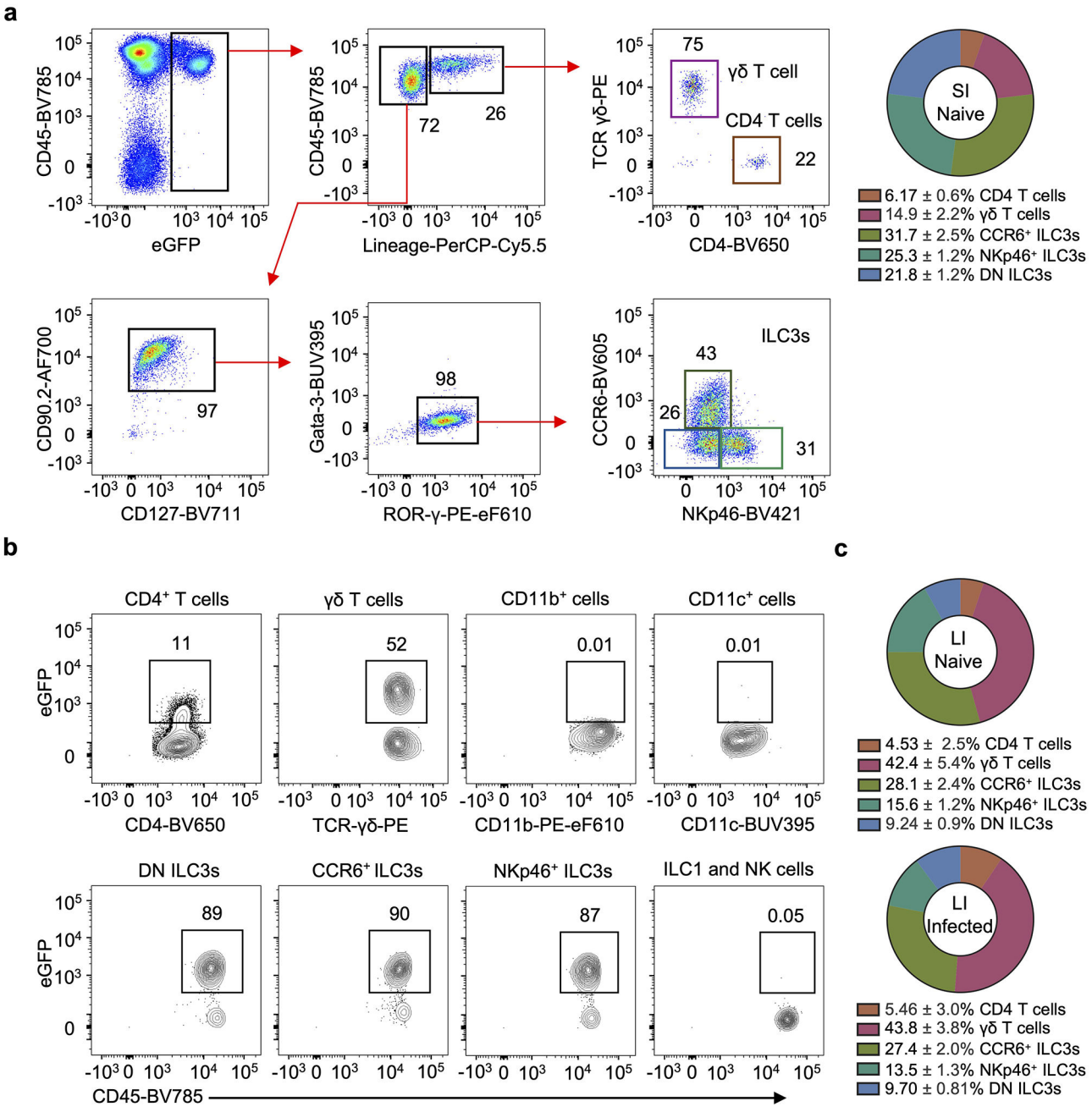

Extended Data Fig. 2 |. Characterization of IL-23R$^+$ immune cells in the intestine.

a, Flow cytometry plots with donut plot of final frequencies of different IL-23R$^+$ immune cells in small intestine lamina propria of IL-23R-eGFP mice (n = 4 mice). Lineage 1, CD11b, CD11c, B220, CD3ε, CD5, CD8α, NK1.1 and TCRγδ. **b,** Flow cytometry plots showing eGFP expression (IL-23R) in different immune cells in small intestine lamina propria of IL-23R-eGFP mice (n = 4 mice). **c,** Donut plots of final frequencies of different IL-23R$^+$ immune cells in large intestine lamina propria of naïve and *C. rodentium* infected

IL-23R-eGFP mice at day 14 post infection (n = 4 mice). Data in **a** and **c** are representative of two or three independent experiments with similar results.

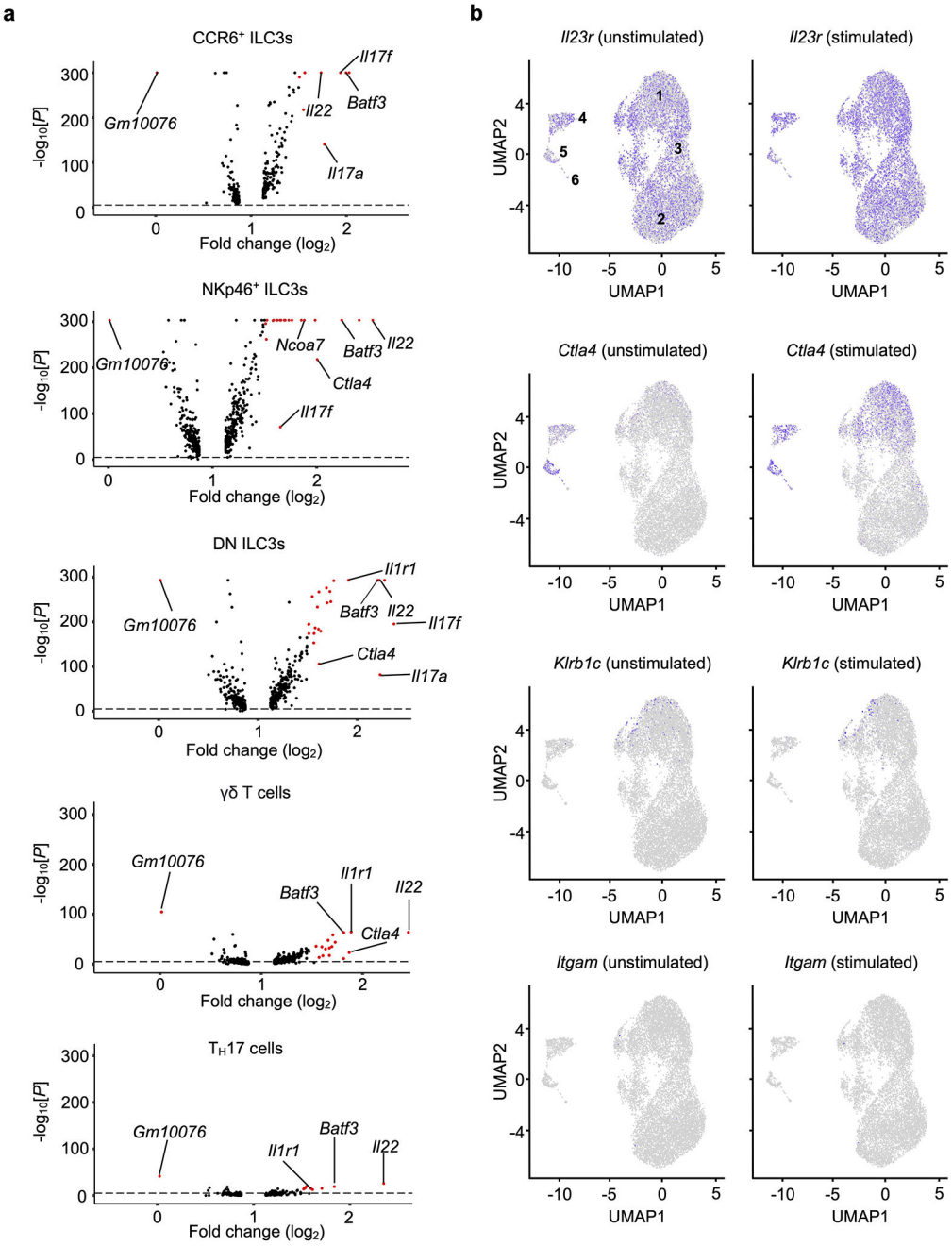

Extended Data Fig. 3 |. Acute IL-23 driven responses in IL-23R$^+$ intestinal cells.
a, Volcano plots of differentially expressed genes in scRNA-seq dataset from IL-23R$^+$ immune cells from the small intestine of IL-23R-eGFP mice before and after IL-23 stimulation in annotated cell types. **b,** UMAP plots of scRNA-seq data showing indicated gene expression in different clusters before and after IL-23 stimulation (1-NKp46$^+$ ILC3s, 2-

CCR6$^+$ ILC3s, 3-DN ILC3s, 4-γδ T cells, 5-T_H17 cells, 6-Proliferative cells). The statistics was obtained by the Wilcoxon test as implemented by Seurat; red dots are significantly different.

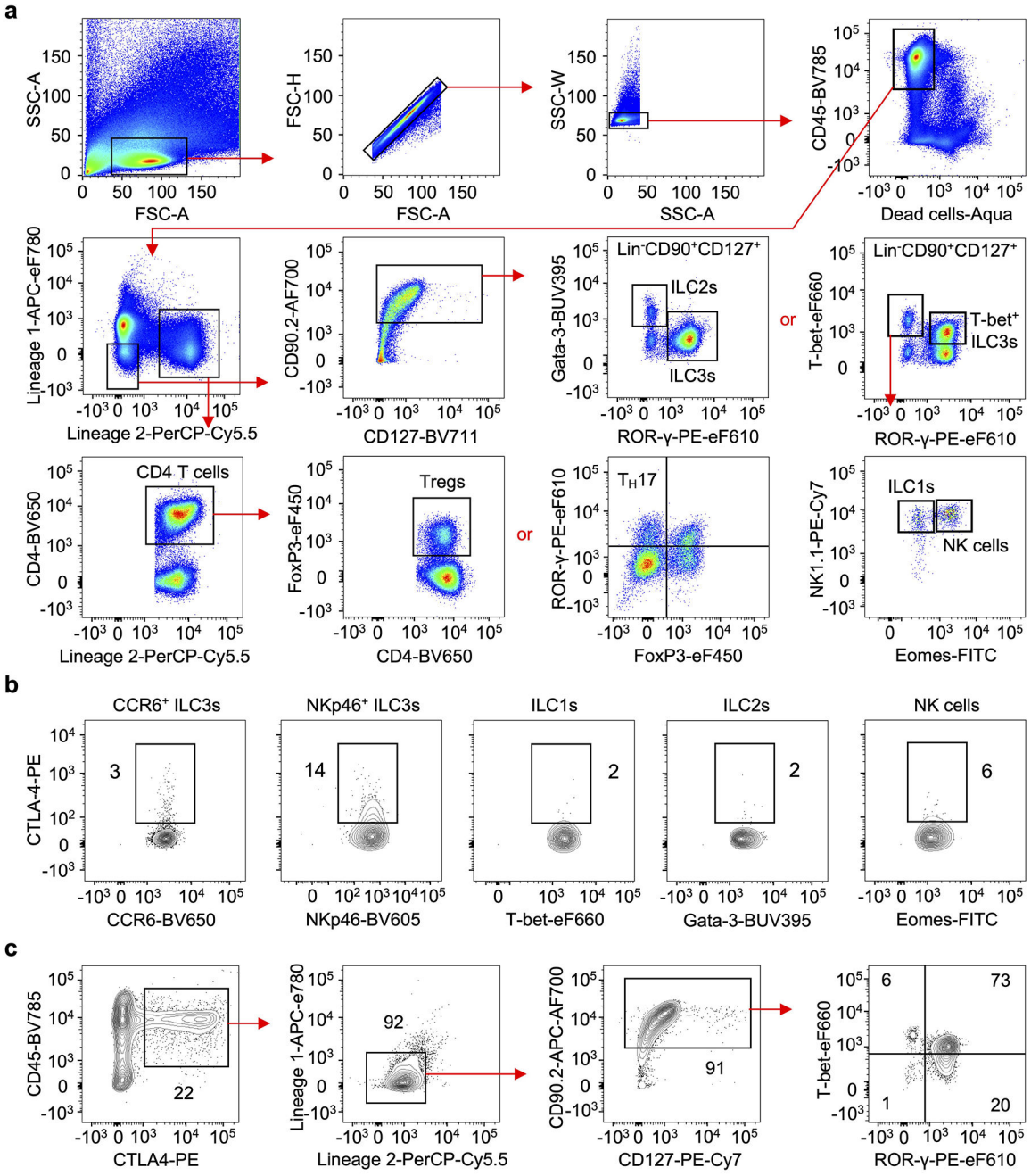

Extended Data Fig. 4 |. Flow cytometry gating for ILCs and CTLA-4.

a, Gating strategy for flow cytometry analysis of different immune cells in intestinal lamina propria of mice. Lineage 1, CD11b, CD11c, F4/80 and B220; lineage 2, CD3ε, CD5, CD8α and TCRγδ; Group 1 innate lymphoid cells (ILC1s) were identified as live CD45$^+$

Lineage$^-$ CD127$^+$ CD90.2$^+$ T-bet$^+$ RORγ^- NK1.1$^+$ Eomes$^-$; group 2 innate lymphoid cells (ILC2s) were identified as live CD45$^+$ Lineage$^-$ CD127$^+$ CD90.2$^+$ GATA3$^+$; group 3 innate lymphoid cells (ILC3s) were identified as live CD45$^+$ Lineage$^-$ CD127$^+$ CD90.2$^+$ RORγ^+; and subsets of ILC3s were further identified as CCR6$^+$ T-bet$^-$ ILC3s or CCR6$^-$ T-bet$^+$ ILC3s. For T cell analysis Tregs were identified as CD45$^+$CD4$^+$FoxP3$^+$ T cells and T_H 17 as CD45$^+$CD4$^+$ RORγ^+FoxP3$^-$ T cells. **b,** Representative flow cytometry plots of CTLA-4 staining in different immune cells from small intestine lamina propria of C57BL/6 mice (n = 4 mice). **c,** Flow cytometry plots of CTLA-4$^+$ cells in small intestine lamina propria of *Rag1*$^{-/-}$ mice (n = 4 mice). Data in **b** and **c** are representative of two independent experiments with similar results.

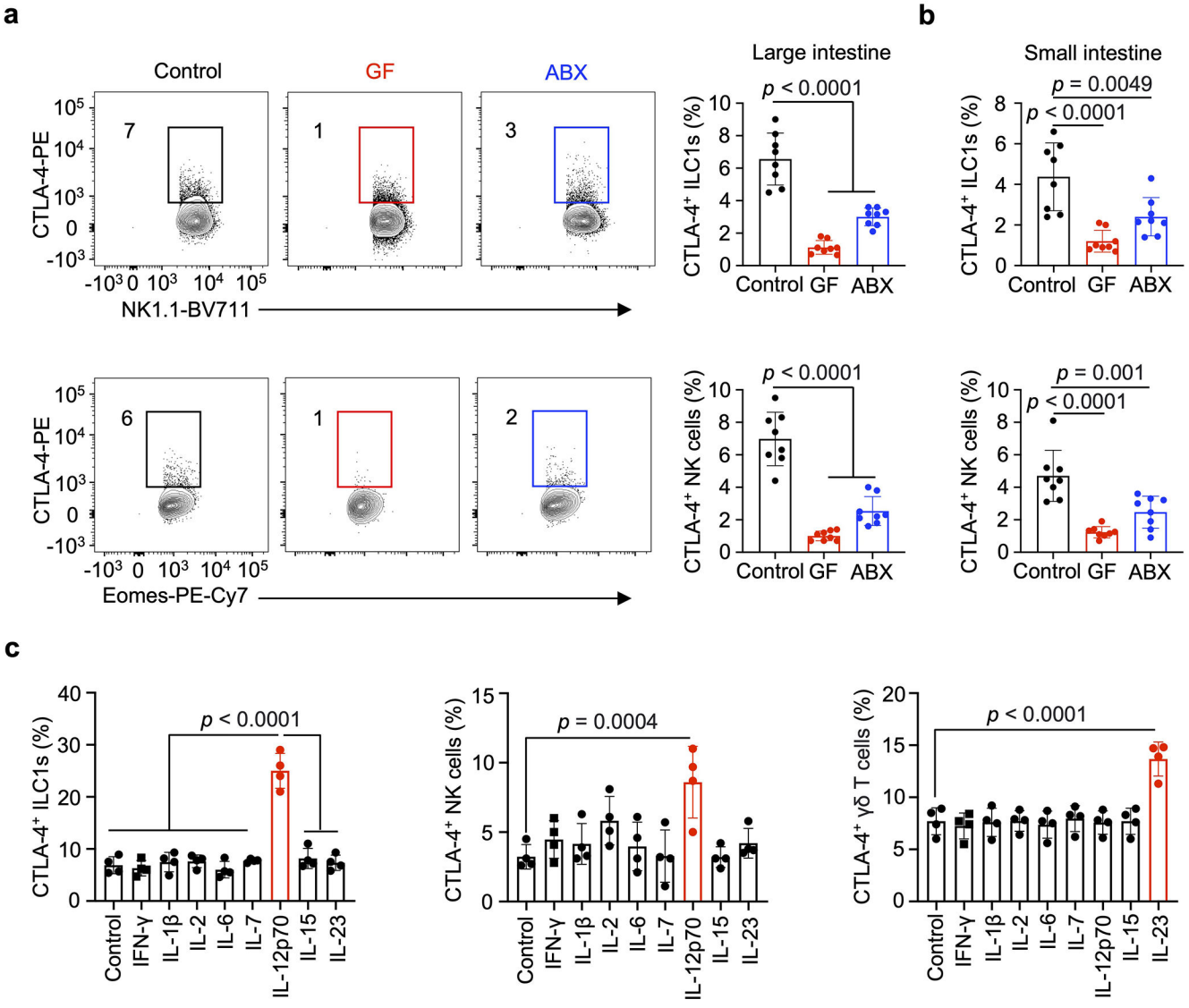

Extended Data Fig. 5 |. Microbiota dependent regulation of CTLA-4.
a, Flow cytometry plots with graph of CTLA-4$^+$ ILC1s and CTLA-4$^+$ NK cells frequencies in large intestine lamina propria of conventional SPF, germ-free (GF) and SPF *Rag1*$^{-/-}$ mice

treated with antibiotics (ABX) ($n = 8$ mice). **b,** Graph of CTLA-4$^+$ ILC1s and CTLA-4$^+$ NK cells frequencies in small intestine lamina propria of conventional SPF, germ-free and SPF mice treated with antibiotics on *Rag1*$^{-/-}$ background ($n = 8$ mice). **c,** Graph of CTLA-4$^+$ ILC1s, CTLA-4$^+$ NK cells and CTLA-4$^+$ γδ T cells frequencies in small intestine lamina propria of SPF mice *ex vivo* stimulated with indicated cytokines ($n = 4$ mice). Data in **a-b** were pooled from two independent experiments and shown as Mean ± s.d.. Data in **c** are representative of two or three independent experiments with similar results and shown as Mean ± s.d.. The statistics in **a-c** were calculated by one-way ANOVA with Dunnett's multiple comparisons.

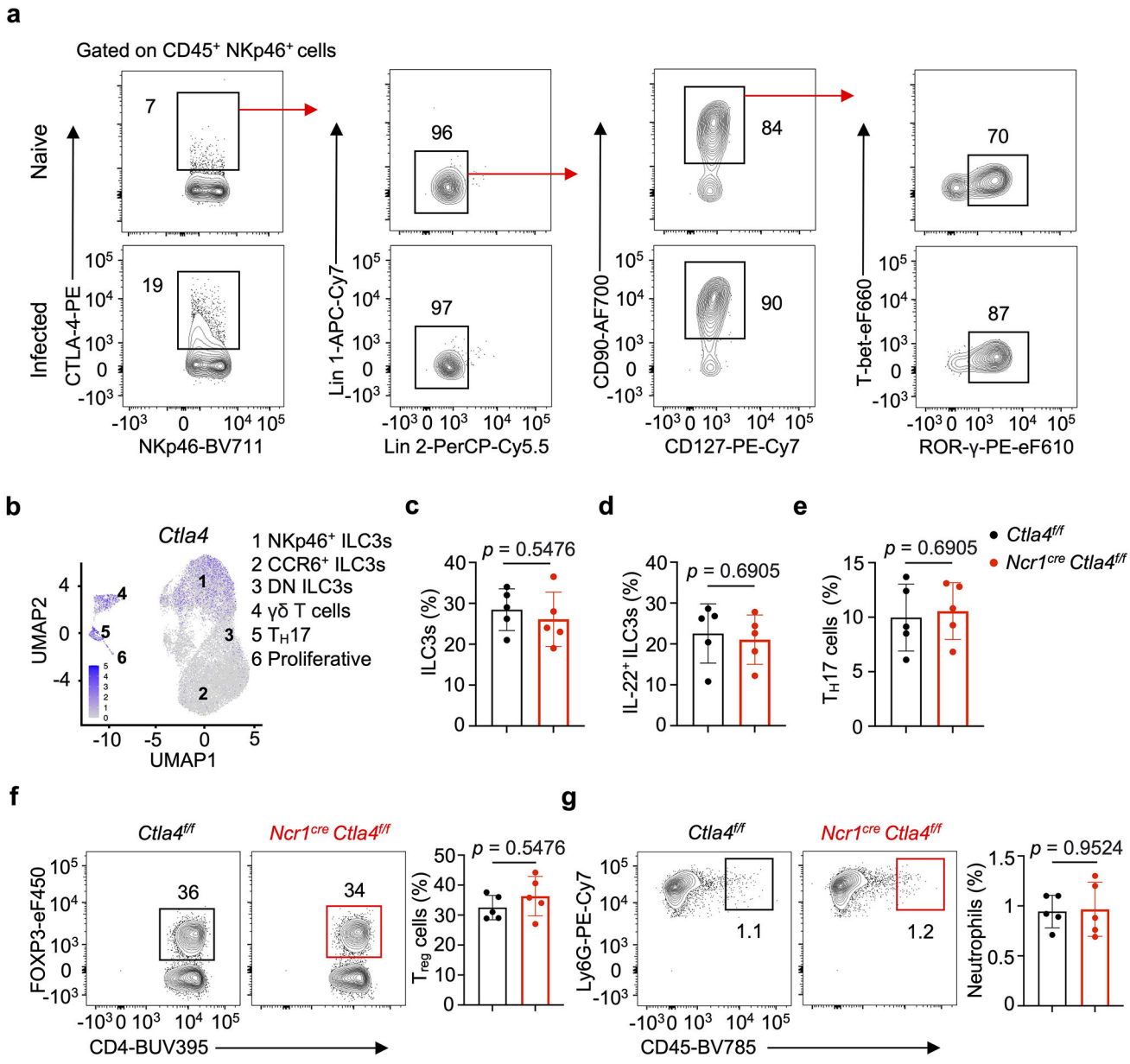

Extended Data Fig. 6 |. Steady state analysis of *Ncr1*^{cre} *Ctla4*$^{f/f}$ mice.

a, Flow cytometry plots of NKp46^{+} cells in large intestine lamina propria of naïve and *C. rodentium* infected C57BL/6 mice (*n* = 4 mice). Lineage 1, CD11b, CD11c and B220; lineage 2, CD3ε, CD5, CD8α, and TCRγδ. **b,** UMAP plot of scRNA-seq data of IL-23R^{+} immune cells from the small intestine of IL-23R-eGFP mice showing *Ctla4* expression in different clusters. The large intestine of *Ncr1*^{cre} *Ctla4*$^{f/f}$ and *Ctla4*$^{f/f}$ were analyzed at steady state and graph displaying the frequency of (**c**) ILC3s (percentage of Lin^{-} CD90^{+} CD127^{+}) and (**d**) IL-22^{+} ILC3s (percentage of total ILC3s). **e,** Graph of T_H17 cells frequency (percentage of CD4^{+} T cells). Flow plots with graph displaying the frequency of (**f**) Treg cells (percentage of CD4^{+} T cells) and (**g**) neutrophils gated as CD11b^{+}Ly6G^{+} cells (percentage of CD45^{+} cells). Data in **a,c,d,e,f** and **g** are representative of two or three independent experiments with similar results (*n* = 5 mice) and shown as Mean ± s.d.. The statistics in **c**-**g** were determined by Mann–Whitney *U*-test (unpaired, two-tailed).

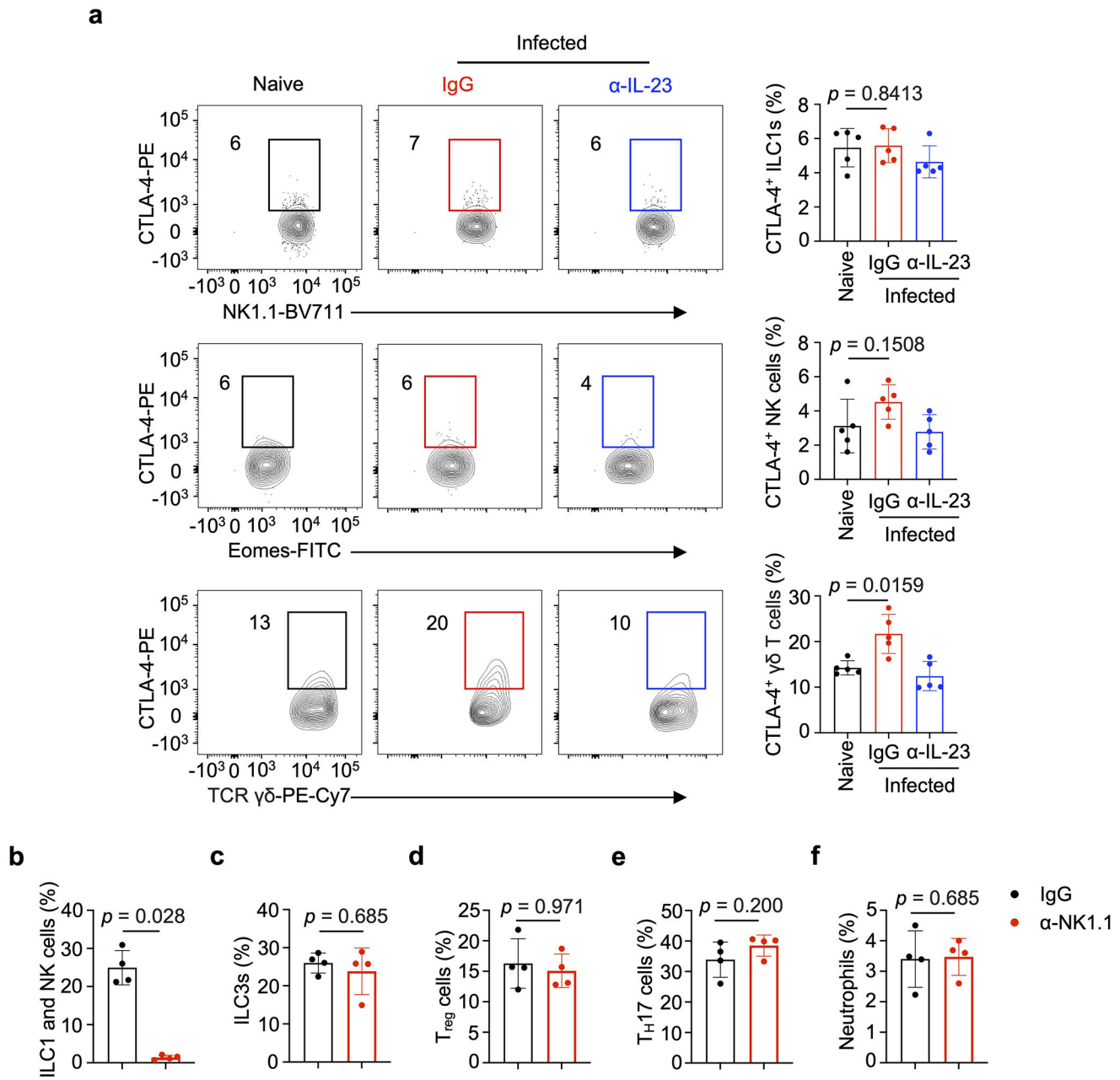

Extended Data Fig. 7 |. NK cells and ILC1s do not impact intestinal inflammation following enteric infection with *C. rodentium*.

C57BL/6 mice were orally infected with *C. rodentium* and treated with IgG or anti-IL-23 monoclonal antibody. **a,** Flow cytometry plots with graph displaying the frequency of CTLA-4 expression on ILC1s, NK cells and γδ T cells *(n* = 5 mice). C57BL/6 mice were orally infected with *C. rodentium* and treated with IgG or anti-NK1.1 monoclonal antibody. Mice were analyzed at day 14 post infection and graph displaying the (**b**) depletion efficiency of natural killer cells and ILC1s, and the frequency of (**c**) ILC3s (percentage of Lin^- $CD90^+$ $CD127^+$); (**d**) Treg cells (percentage of $CD4^+$ T cells); (**e**) T_H17 cells (percentage of $CD4^+$ T cells); (**f**) Neutrophils gated as $CD11b^+Ly6G^+$ cells (percentage of

CD45$^+$ cells) in large intestinal lamina propria immune cells. Data in **b-f** are representative of two or three independent experiments with similar results (*n* = 4 mice) and shown as Mean ± s.d.. The statistics in **a-f** were determined by Mann–Whitney *U*-test (unpaired, two-tailed).

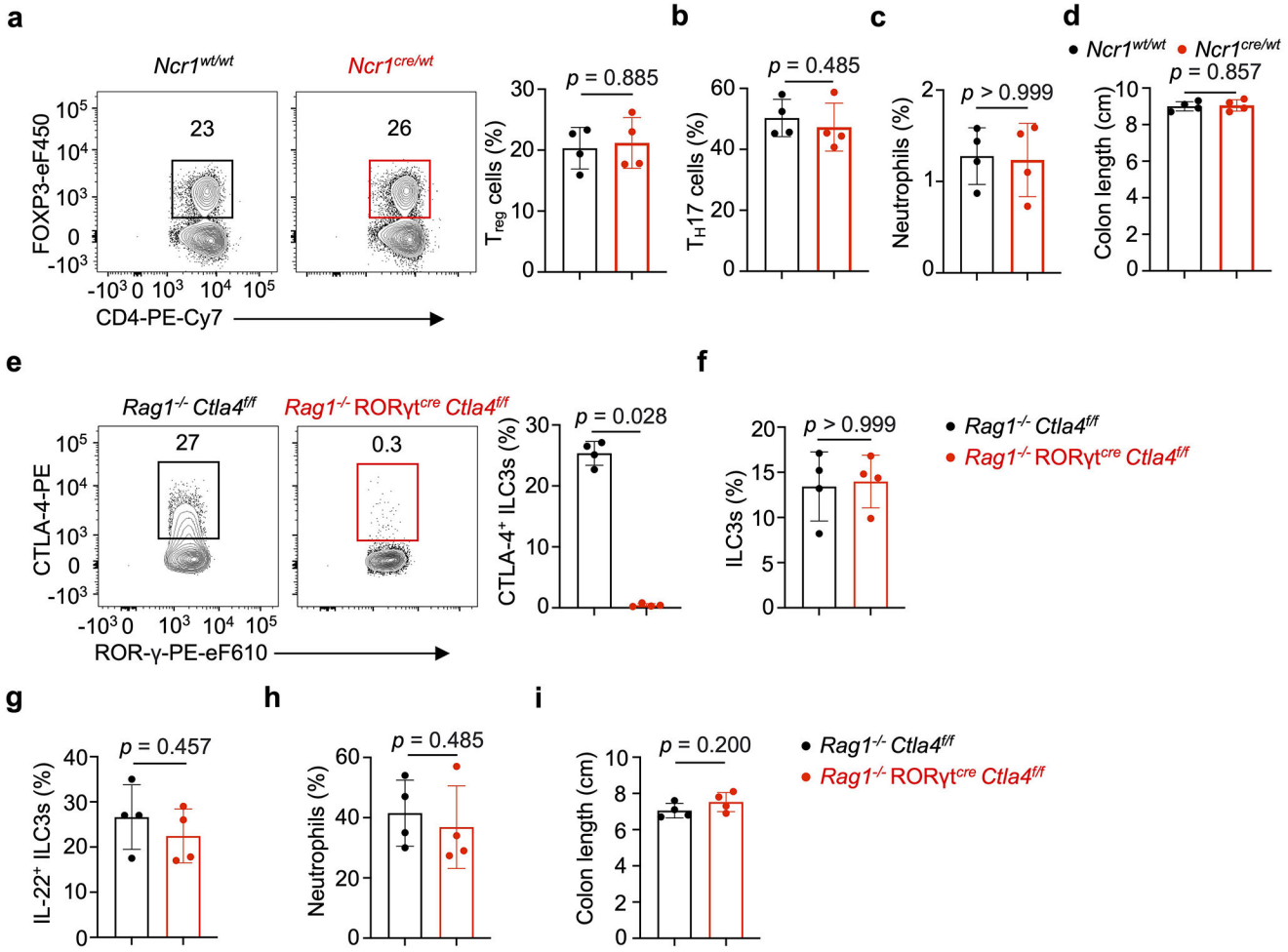

Extended Data Fig. 8 |. Innate immune responses are intact in mice lacking ILC3-specific CTLA-4.

Ncr1$^{wt/wt}$ and Ncr1$^{cre/wt}$ mice were orally infected with *C. rodentium* and at day 14 post infection large intestinal lamina propria immune cells were analyzed. **a,** Flow cytometry plots with graph of Tregs frequency (percentage of CD4$^+$ T cells) and graph displaying the frequency of (**b**) T_H17 cells (percentage of CD4$^+$ T cells) and (**c**) neutrophils gated as CD11b$^+$Ly6G$^+$ cells (percentage of CD45$^+$ cells) with (**d**) colon length. **e,** Flow cytometry plots and graph of CTLA-4$^+$ ILC3s frequency (percentage of total ILC3s) in *Rag1$^{-/-}$ Ctla4$^{f/f}$ and Rag1$^{-/-}$* RORγt^{cre} *Ctla4$^{f/f}$* mice. *Rag1$^{-/-}$ Ctla4$^{f/f}$ and Rag1$^{-/-}$* RORγt^{cre} *Ctla4$^{f/f}$* mice were treated with 100 μg of anti-CD40 antibody, and graph displaying the frequency of (**f**) ILC3s (percentage of Lin$^-$ CD90$^+$ CD127$^+$); (**g**) IL-22$^+$ ILC3s (percentage of total ILC3s) and (**h**) neutrophils gated as CD11b$^+$Ly6G$^+$ cells (percentage of CD45$^+$ cells) in the large intestines with (**i**) colon length at day 7 post treatment. Data in **a-i** are representative of two

independent experiments with similar results ($n = 4$ mice) and shown as Mean ± s.d.. The statistics in **a-i** were determined by Mann–Whitney *U*-test (unpaired, two-tailed).

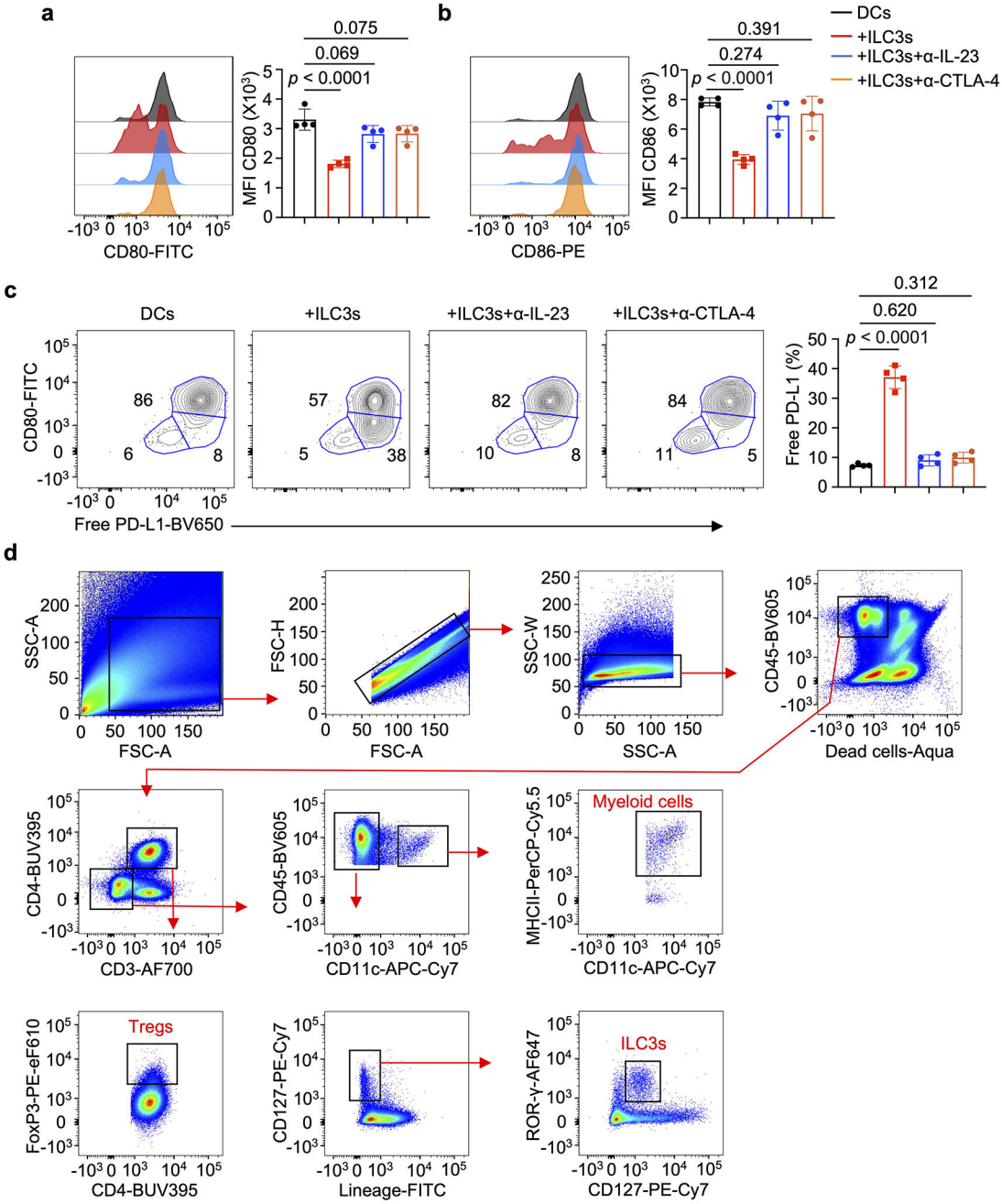

Extended Data Fig. 9 |. CTLA-4$^+$ ILC3s reduce co-stimulatory molecules and enhance PD-L1 on myeloid cells in response to IL-23.

Sorted ILC3s and myeloid cells from the large intestine of C57BL/6 mice were co-cultured with recombinant IL-23 in presence or absence of indicated blocking antibodies. Flow cytometry plots with graph of MFI of (**a**) CD80 and (**b**) CD86 expression on myeloid cells gated as CD11c$^+$ MHCII^{hi}. **c,** Flow cytometry plots with graph of free PD-L1 frequency on

myeloid cells gated as CD11c^{+} MHCII^{hi}. **d,** Gating strategy to analyze T cells, myeloid cells and ILC3s in human samples. Data in **a-c** are representative of two independent experiments with similar results (*n* = 4 mice) and shown as Mean ± s.d.. The statistics were calculated by one-way ANOVA with Dunnett's multiple comparisons.

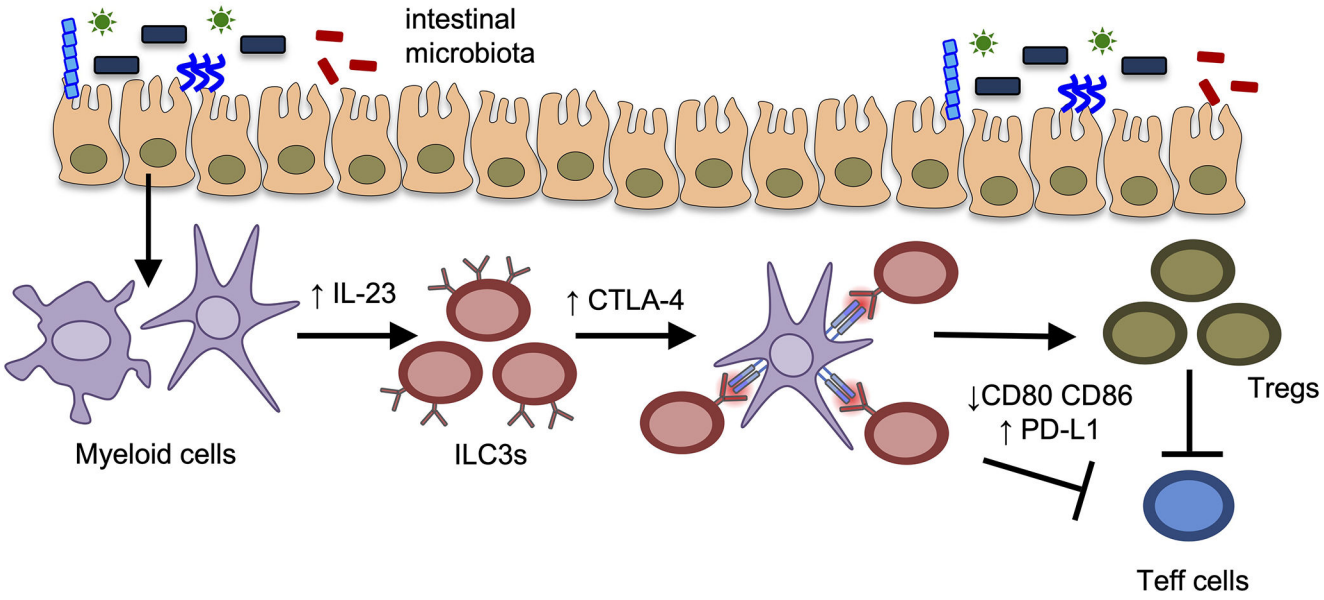

Extended Data Fig. 10 |. ILC3s restrain IL-23 mediated inflammation through CTLA-4.
Here we define a pathway of immune regulation in the large intestine. This pathway is activated by gut microbes and IL-23 in a FOXO1- and STAT3-dependent manner. ILC3-intrinsic CTLA-4 shapes the levels of co-inhibitory and co-stimulatory molecules on intestinal myeloid cells to support Tregs and restrict T effector (Teff) cells. Consequently, ILC3-intrinsic CTLA-4 function as a checkpoint to restrain the pathologic functions of IL-23, suggesting that disruption of these lymphocytes, which occurs in IBD, contributes to chronic inflammation.

Supplementary Material

Refer to Web version on PubMed Central for supplementary material.

Acknowledgements

We thank members of the Sonnenberg Laboratory for discussions and critical reading of the manuscript. Research in the Sonnenberg Laboratory is supported by the National Institutes of Health (R01AI143842, R01AI123368, R01AI145989, U01AI095608, R01AI162936, R01CA274534, and R37AI174468), an Investigators in the Pathogenesis of Infectious Disease Award from the Burroughs Wellcome Fund, the Meyer Cancer Center Collaborative Research Initiative, the Dalton Family Foundation, and Linda and Glenn Greenberg. A.A. and M.L. are supported by fellowships from the Crohn's and Colitis Foundation (902451 and 935259). A.M.J and J.U. are supported by NIH T32DK116970. J.Z. is supported by F32DK136248. V.H. is supported by a DFG Walter Benjamin Fellowship (HO 7399/1-1). G.F.S. is a CRI Lloyd J. Old STAR. We would like to thank the Epigenomics Cores of Weill Cornell Medicine, N. Zahan for administrative support, and D. Garone and A. Brcic-Susak for technical support. The JRI Live Cell Bank is supported by the JRI, Jill Roberts Center for IBD, Cure for IBD, the Rosanne H. Silbermann Foundation, the Sanders Family, and Weill Cornell Medicine Division of Pediatric Gastroenterology and Nutrition.

Data availability.

All data necessary to understand and evaluate the conclusions of this paper are provided. Single cell RNA sequencing data has been deposited in the Gene Expression Omnibus database under the accession number GSE229976. Bulk RNA sequencing RNA sequencing data has been deposited under the accession number GSE247742.

References

1. Abraham C & Cho JH IL-23 and autoimmunity: new insights into the pathogenesis of inflammatory bowel disease. Annu Rev Med 60, 97–110 (2009). 10.1146/annurev.med.60.051407.123757 [PubMed: 18976050]
2. Maloy KJ & Powrie F Intestinal homeostasis and its breakdown in inflammatory bowel disease. Nature 474, 298–306 (2011). 10.1038/nature10208 [PubMed: 21677746]
3. Maynard CL, Elson CO, Hatton RD & Weaver CT Reciprocal interactions of the intestinal microbiota and immune system. Nature 489, 231–241 (2012). 10.1038/nature11551 [PubMed: 22972296]
4. Fragoulis GE, Siebert S & McInnes IB Therapeutic Targeting of IL-17 and IL-23 Cytokines in Immune-Mediated Diseases. Annu Rev Med 67, 337–353 (2016). 10.1146/annurev-med-051914-021944 [PubMed: 26565676]
5. Bernink JH et al. Human type 1 innate lymphoid cells accumulate in inflamed mucosal tissues. Nat Immunol 14, 221–229 (2013). 10.1038/ni.2534 [PubMed: 23334791]
6. Takayama T et al. Imbalance of NKp44(+)NKp46(−) and NKp44(−)NKp46(+) natural killer cells in the intestinal mucosa of patients with Crohn's disease. Gastroenterology 139, 882–892, 892.e881–883 (2010). 10.1053/j.gastro.2010.05.040 [PubMed: 20638936]
7. Zhou L et al. Innate lymphoid cells support regulatory T cells in the intestine through interleukin-2. Nature 568, 405–409 (2019). 10.1038/s41586-019-1082-x [PubMed: 30944470]
8. Oppmann B et al. Novel p19 protein engages IL-12p40 to form a cytokine, IL-23, with biological activities similar as well as distinct from IL-12. Immunity 13, 715–725 (2000). 10.1016/s1074-7613(00)00070-4 [PubMed: 11114383]
9. Neurath MF IL-23: a master regulator in Crohn disease. Nat Med 13, 26–28 (2007). 10.1038/nm0107-26 [PubMed: 17206128]
10. Krueger GG et al. A human interleukin-12/23 monoclonal antibody for the treatment of psoriasis. N Engl J Med 356, 580–592 (2007). 10.1056/NEJMoa062382 [PubMed: 17287478]
11. Lubberts E The IL-23-IL-17 axis in inflammatory arthritis. Nat Rev Rheumatol 11, 415–429 (2015). 10.1038/nrrheum.2015.53 [PubMed: 25907700]
12. Cua DJ et al. Interleukin-23 rather than interleukin-12 is the critical cytokine for autoimmune inflammation of the brain. Nature 421, 744–748 (2003). 10.1038/nature01355 [PubMed: 12610626]
13. Duerr RH et al. A genome-wide association study identifies IL23R as an inflammatory bowel disease gene. Science 314, 1461–1463 (2006). 10.1126/science.1135245 [PubMed: 17068223]
14. Consortium WTCC Genome-wide association study of 14,000 cases of seven common diseases and 3,000 shared controls. Nature 447, 661–678 (2007). 10.1038/nature05911 [PubMed: 17554300]
15. D'Haens G et al. Risankizumab as induction therapy for Crohn's disease: results from the phase 3 ADVANCE and MOTIVATE induction trials. Lancet 399, 2015–2030 (2022). 10.1016/S0140-6736(22)00467-6 [PubMed: 35644154]
16. Feagan BG et al. Ustekinumab as Induction and Maintenance Therapy for Crohn's Disease. N Engl J Med 375, 1946–1960 (2016). 10.1056/NEJMoa1602773 [PubMed: 27959607]
17. Sands BE et al. Ustekinumab as Induction and Maintenance Therapy for Ulcerative Colitis. N Engl J Med 381, 1201–1214 (2019). 10.1056/NEJMoa1900750 [PubMed: 31553833]

18. Shih VF et al. Homeostatic IL-23 receptor signaling limits Th17 response through IL-22-mediated containment of commensal microbiota. Proc Natl Acad Sci U S A 111, 13942–13947 (2014). 10.1073/pnas.1323852111 [PubMed: 25201978]
19. Mangan PR et al. Transforming growth factor-beta induces development of the T(H)17 lineage. Nature 441, 231–234 (2006). 10.1038/nature04754 [PubMed: 16648837]
20. Zheng Y et al. Interleukin-22 mediates early host defense against attaching and effacing bacterial pathogens. Nat Med 14, 282–289 (2008). 10.1038/nm1720 [PubMed: 18264109]
21. Sonnenberg GF, Monticelli LA, Elloso MM, Fouser LA & Artis D CD4(+) lymphoid tissue-inducer cells promote innate immunity in the gut. Immunity 34, 122–134 (2011). 10.1016/j.immuni.2010.12.009 [PubMed: 21194981]
22. Cox JH et al. Opposing consequences of IL-23 signaling mediated by innate and adaptive cells in chemically induced colitis in mice. Mucosal Immunol 5, 99–109 (2012). 10.1038/mi.2011.54 [PubMed: 22089030]
23. Izcue A et al. Interleukin-23 restrains regulatory T cell activity to drive T cell-dependent colitis. Immunity 28, 559–570 (2008). 10.1016/j.immuni.2008.02.019 [PubMed: 18400195]
24. Martínez-Barricarte R et al. Human IFN-γ immunity to mycobacteria is governed by both IL-12 and IL-23. Sci Immunol 3 (2018). 10.1126/sciimmunol.aau6759
25. Mao K et al. Innate and adaptive lymphocytes sequentially shape the gut microbiota and lipid metabolism. Nature 554, 255–259 (2018). 10.1038/nature25437 [PubMed: 29364878]
26. Sawa S et al. RORγt+ innate lymphoid cells regulate intestinal homeostasis by integrating negative signals from the symbiotic microbiota. Nat Immunol 12, 320–326 (2011). 10.1038/ni.2002 [PubMed: 21336274]
27. Sonnenberg GF & Artis D Innate lymphoid cells in the initiation, regulation and resolution of inflammation. Nat Med 21, 698–708 (2015). 10.1038/nm.3892 [PubMed: 26121198]
28. Spits H et al. Innate lymphoid cells--a proposal for uniform nomenclature. Nat Rev Immunol 13, 145–149 (2013). 10.1038/nri3365 [PubMed: 23348417]
29. Kerdiles YM et al. Foxo transcription factors control regulatory T cell development and function. Immunity 33, 890–904 (2010). 10.1016/j.immuni.2010.12.002 [PubMed: 21167754]
30. Hossain DM et al. FoxP3 acts as a cotranscription factor with STAT3 in tumor-induced regulatory T cells. Immunity 39, 1057–1069 (2013). 10.1016/j.immuni.2013.11.005 [PubMed: 24315995]
31. Jacobse J et al. Interleukin-23 receptor signaling impairs the stability and function of colonic regulatory T cells. Cell Rep 42, 112128 (2023). 10.1016/j.celrep.2023.112128 [PubMed: 36807140]
32. Kannan AK et al. IL-23 induces regulatory T cell plasticity with implications for inflammatory skin diseases. Sci Rep 9, 17675 (2019). 10.1038/s41598-019-53240-z [PubMed: 31776355]
33. Uhlig HH et al. Differential activity of IL-12 and IL-23 in mucosal and systemic innate immune pathology. Immunity 25, 309–318 (2006). 10.1016/j.immuni.2006.05.017 [PubMed: 16919486]
34. Ahern PP et al. Interleukin-23 drives intestinal inflammation through direct activity on T cells. Immunity 33, 279–288 (2010). 10.1016/j.immuni.2010.08.010 [PubMed: 20732640]
35. Wing K et al. CTLA-4 control over Foxp3+ regulatory T cell function. Science 322, 271–275 (2008). 10.1126/science.1160062 [PubMed: 18845758]
36. Walker LS & Sansom DM The emerging role of CTLA4 as a cell-extrinsic regulator of T cell responses. Nat Rev Immunol 11, 852–863 (2011). 10.1038/nri3108 [PubMed: 22116087]
37. Chang TT, Jabs C, Sobel RA, Kuchroo VK & Sharpe AH Studies in B7-deficient mice reveal a critical role for B7 costimulation in both induction and effector phases of experimental autoimmune encephalomyelitis. J Exp Med 190, 733–740 (1999). 10.1084/jem.190.5.733 [PubMed: 10477557]
38. Lenschow DJ et al. CD28/B7 regulation of Th1 and Th2 subsets in the development of autoimmune diabetes. Immunity 5, 285–293 (1996). 10.1016/s1074-7613(00)80323-4 [PubMed: 8808683]
39. Tekguc M, Wing JB, Osaki M, Long J & Sakaguchi S Treg-expressed CTLA-4 depletes CD80/CD86 by trogocytosis, releasing free PD-L1 on antigen-presenting cells. Proc Natl Acad Sci U S A 118 (2021). 10.1073/pnas.2023739118

40. Sugiura D et al. Restriction of PD-1 function by cis-PD-L1/CD80 interactions is required for optimal T cell responses. Science 364, 558–566 (2019). 10.1126/science.aav7062 [PubMed: 31000591]
41. Francisco LM et al. PD-L1 regulates the development, maintenance, and function of induced regulatory T cells. J Exp Med 206, 3015–3029 (2009). 10.1084/jem.20090847 [PubMed: 20008522]
42. Keir ME et al. Tissue expression of PD-L1 mediates peripheral T cell tolerance. J Exp Med 203, 883–895 (2006). 10.1084/jem.20051776 [PubMed: 16606670]
43. Lyu M et al. ILC3s select microbiota-specific regulatory T cells to establish tolerance in the gut. Nature 610, 744–751 (2022). 10.1038/s41586-022-05141-x [PubMed: 36071169]
44. Paustian AMS et al. Continuous IL-23 stimulation drives ILC3 depletion in the upper GI tract and, in combination with TNFα, induces robust activation and a phenotypic switch of ILC3. PLoS One 12, e0182841 (2017). 10.1371/journal.pone.0182841 [PubMed: 28792532]
45. Jacquelot N et al. Immune Checkpoints and Innate Lymphoid Cells-New Avenues for Cancer Immunotherapy. Cancers (Basel) 13 (2021). 10.3390/cancers13235967
46. Hepworth MR et al. Immune tolerance. Group 3 innate lymphoid cells mediate intestinal selection of commensal bacteria-specific $CD4^+$ T cells. Science 348, 1031–1035 (2015). 10.1126/science.aaa4812 [PubMed: 25908663]
47. Goc J et al. Dysregulation of ILC3s unleashes progression and immunotherapy resistance in colon cancer. Cell 184, 5015–5030.e5016 (2021). 10.1016/j.cell.2021.07.029 [PubMed: 34407392]
48. Kløverpris HN et al. Innate Lymphoid Cells Are Depleted Irreversibly during Acute HIV-1 Infection in the Absence of Viral Suppression. Immunity 44, 391–405 (2016). 10.1016/j.immuni.2016.01.006 [PubMed: 26850658]
49. Page DB, Postow MA, Callahan MK, Allison JP & Wolchok JD Immune modulation in cancer with antibodies. Annu Rev Med 65, 185–202 (2014). 10.1146/annurev-med-092012-112807 [PubMed: 24188664]
50. Lo BC et al. Microbiota-dependent activation of CD4+ T cells induces CTLA-4 blockade-associated colitis via Fcγ receptors. Science 383, 62–70 (2024). 10.1126/science.adh8342 [PubMed: 38175892]
51. Mombaerts P et al. RAG-1-deficient mice have no mature B and T lymphocytes. Cell 68, 869–877 (1992). 10.1016/0092-8674(92)90030-g [PubMed: 1547488]
52. Kühn R, Löhler J, Rennick D, Rajewsky K & Müller W Interleukin-10-deficient mice develop chronic enterocolitis. Cell 75, 263–274 (1993). 10.1016/0092-8674(93)80068-p [PubMed: 8402911]
53. Awasthi A et al. Cutting edge: IL-23 receptor gfp reporter mice reveal distinct populations of IL-17-producing cells. J Immunol 182, 5904–5908 (2009). 10.4049/jimmunol.0900732 [PubMed: 19414740]
54. Lochner M et al. In vivo equilibrium of proinflammatory IL-17+ and regulatory IL-10+ Foxp3+ RORgamma t+ T cells. J Exp Med 205, 1381–1393 (2008). 10.1084/jem.20080034 [PubMed: 18504307]
55. Narni-Mancinelli E et al. Fate mapping analysis of lymphoid cells expressing the NKp46 cell surface receptor. Proc Natl Acad Sci U S A 108, 18324–18329 (2011). 10.1073/pnas.1112064108 [PubMed: 22021440]
56. Butler A, Hoffman P, Smibert P, Papalexi E & Satija R Integrating single-cell transcriptomic data across different conditions, technologies, and species. Nat Biotechnol 36, 411–420 (2018). 10.1038/nbt.4096 [PubMed: 29608179]

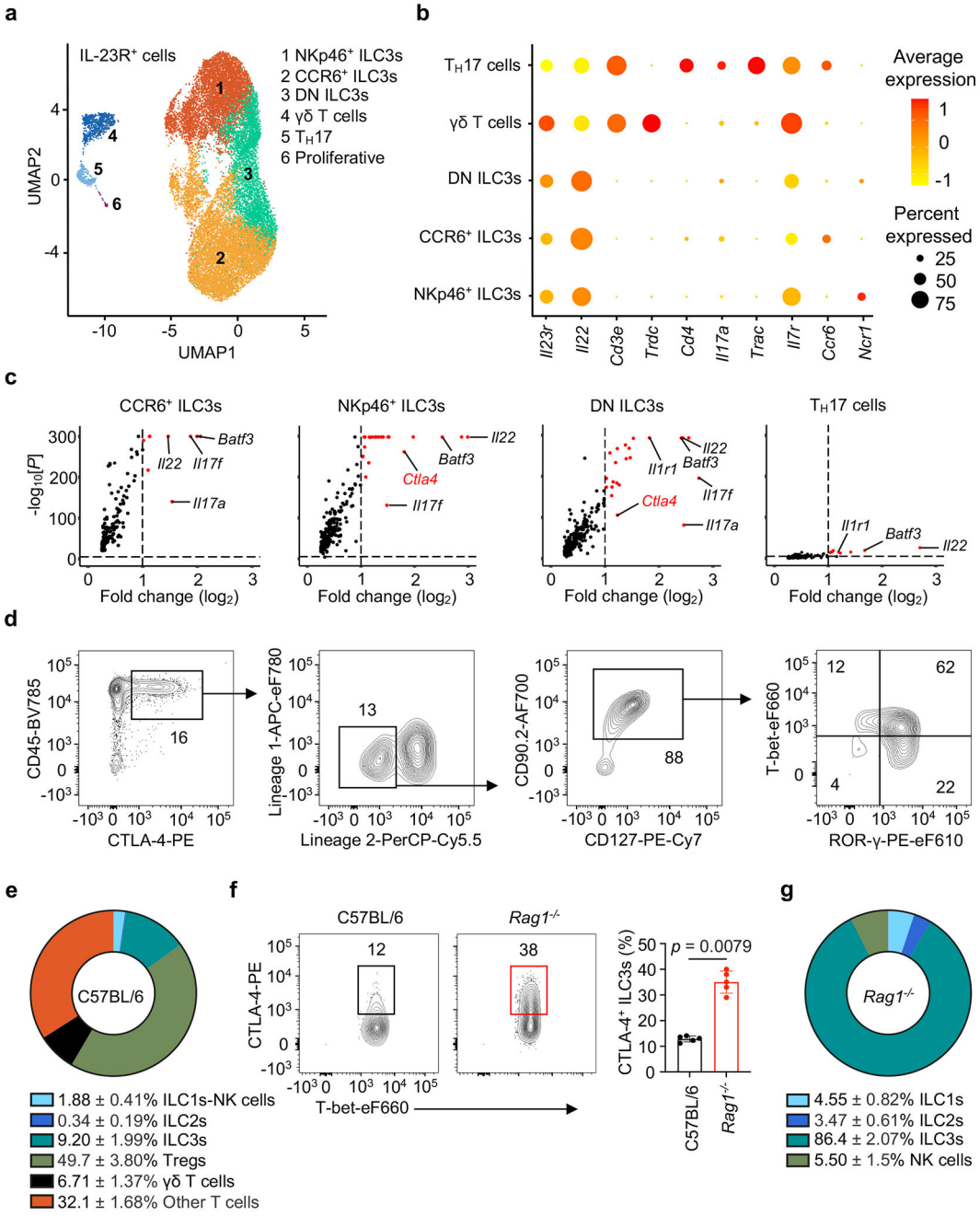

Figure 1 |. A single cell atlas of IL-23 responses in the small intestine identifies CTLA-4$^+$ ILC3s.

a, UMAP plot of scRNA-seq data encompassing IL-23R$^+$ immune cells from small intestine lamina propria of IL-23R-eGFP mice. DN, double-negative. **b**, Dot plots showing the mean expression of the indicated genes among different clusters. **c**, Volcano plots of differentially expressed genes in scRNA-seq dataset of IL-23R$^+$ immune cells from small intestine lamina propria of IL-23R-eGFP mice before or after IL-23 stimulation. **d**, Flow cytometry plots and (**e**) donut plot with final frequencies of different CTLA-4$^+$ cells in small intestine lamina propria of C57BL/6 mice (n = 4 mice). Lineage 1, CD11b, CD11c and B220; lineage

2, CD3ε, CD5, CD8α, and TCRγδ. **f,** Flow cytometry plots with graph displaying the frequency of CTLA-4^{+} ILC3s (percentage of total ILC3s) in small intestine lamina propria of C57BL/6 and *Rag1*$^{-/-}$ mice (n = 5 mice). **g,** Donut plot with final frequencies of different CTLA-4^{+} cells in small intestine lamina propria of *Rag1*$^{-/-}$ mice (n = 4 mice). Data in **d**-**g** are representative of two or three independent experiments with similar results, shown as mean ± s.d. The statistics in **c** were obtained by the Wilcoxon test as implemented by Seurat. The Statistic in **f** was calculated by Mann–Whitney *U*-test (unpaired, two-tailed).

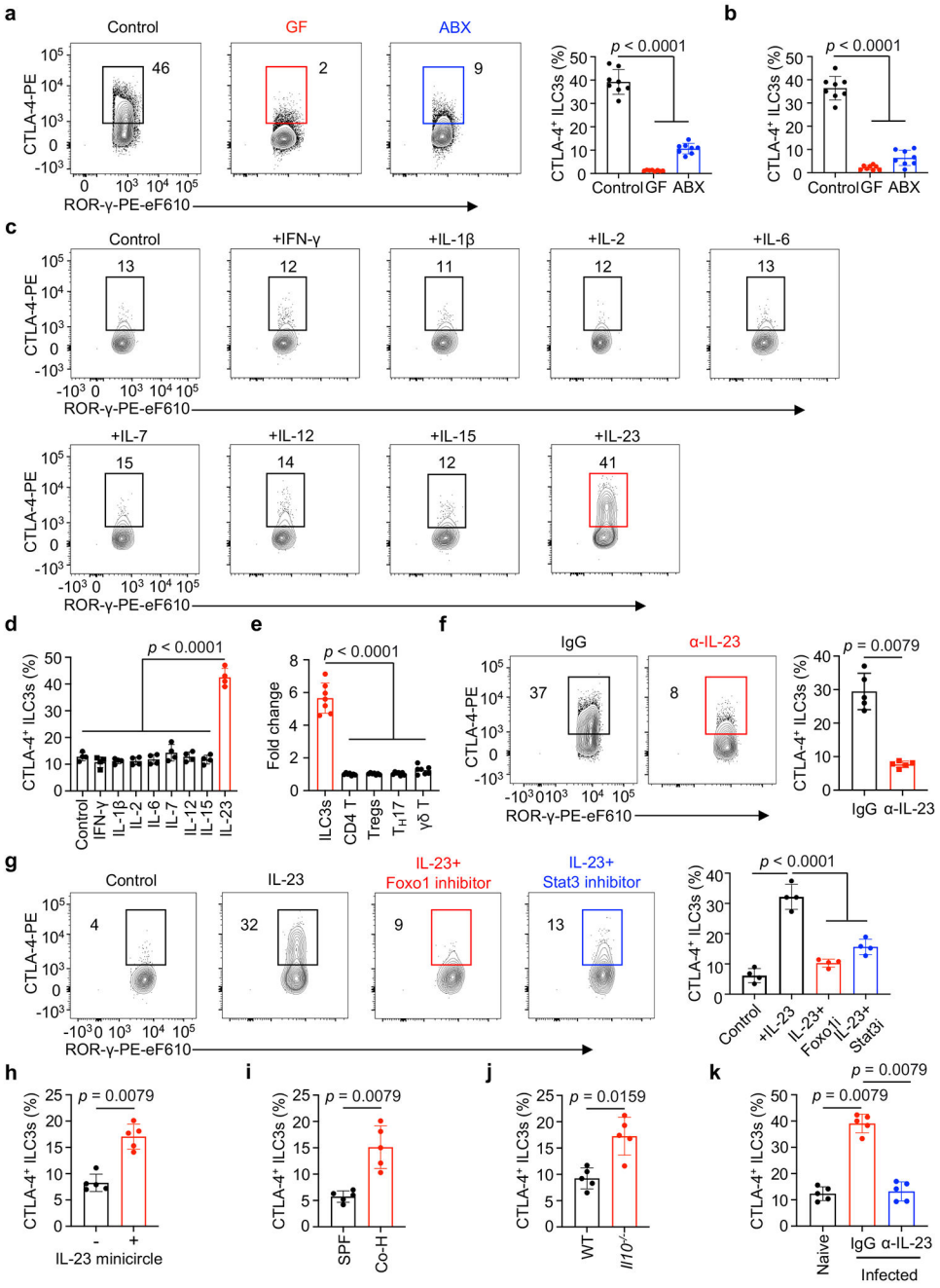

Figure 2 |. Microbial exposure elicits IL-23 to upregulate CTLA-4 on ILC3s.

Flow cytometry plots with graph of CTLA-4^{+} ILC3 frequency (percentage of total ILC3s) in (**a**) large intestine and (**b**) small intestine lamina propria of SPF, germ-free (GF) and SPF *Rag1*$^{-/-}$ mice treated with antibiotics (ABX) (n = 8 mice). **c,** Flow cytometry plots and (**d**) graph of CTLA-4^{+} ILC3 frequency (percentage of total ILC3s) in small intestine lamina propria of SPF mice *ex vivo* stimulated with indicated cytokines (n = 4 mice). **e,** Fold change in CTLA-4 protein in different immune cells from lamina propria of SPF mice *ex vivo* cultured for 4 hours with IL-23 (n = 7 mice). **f,** Flow cytometry plots with graph

of CTLA-4^{+} ILC3 frequency (percentage of total ILC3s) in small intestine lamina propria of *Rag1*$^{-/-}$ mice treated with IgG control or anti-IL-23 antibody (n = 5 mice). **g,** Flow cytometry plots of CTLA-4^{+} ILC3s (percentage of total ILC3s) in small intestine lamina propria of SPF mice cultured *ex vivo* in different conditions (n = 4 mice). Graphs showing frequency of CTLA-4^{+} ILC3s (percentage of total ILC3s) in large intestine lamina propria of (**h**) mice injected with or without IL-23 minicircle; (**i**) SPF mice co-housed (Co-H) with or without pet store mice; (**j**) C57BL/6 WT and *Il10*$^{-/-}$ mice; or (**k**) mice infected with *C. rodentium* treated with IgG control or anti-IL-23 antibody (n = 5 mice). Data in **a,b** and **e** were pooled from two independent experiments with similar results, shown as Mean ± s.d.. Data in **c,d** and **f-k** are representative of two independent experiments, shown as mean ± s.d. The statistics in **a,b,d,e** and **g** were calculated by one-way ANOVA with Dunnett's multiple comparisons. The statistics in **f** and **h-k** were calculated by Mann–Whitney *U*-test (unpaired, two-tailed).

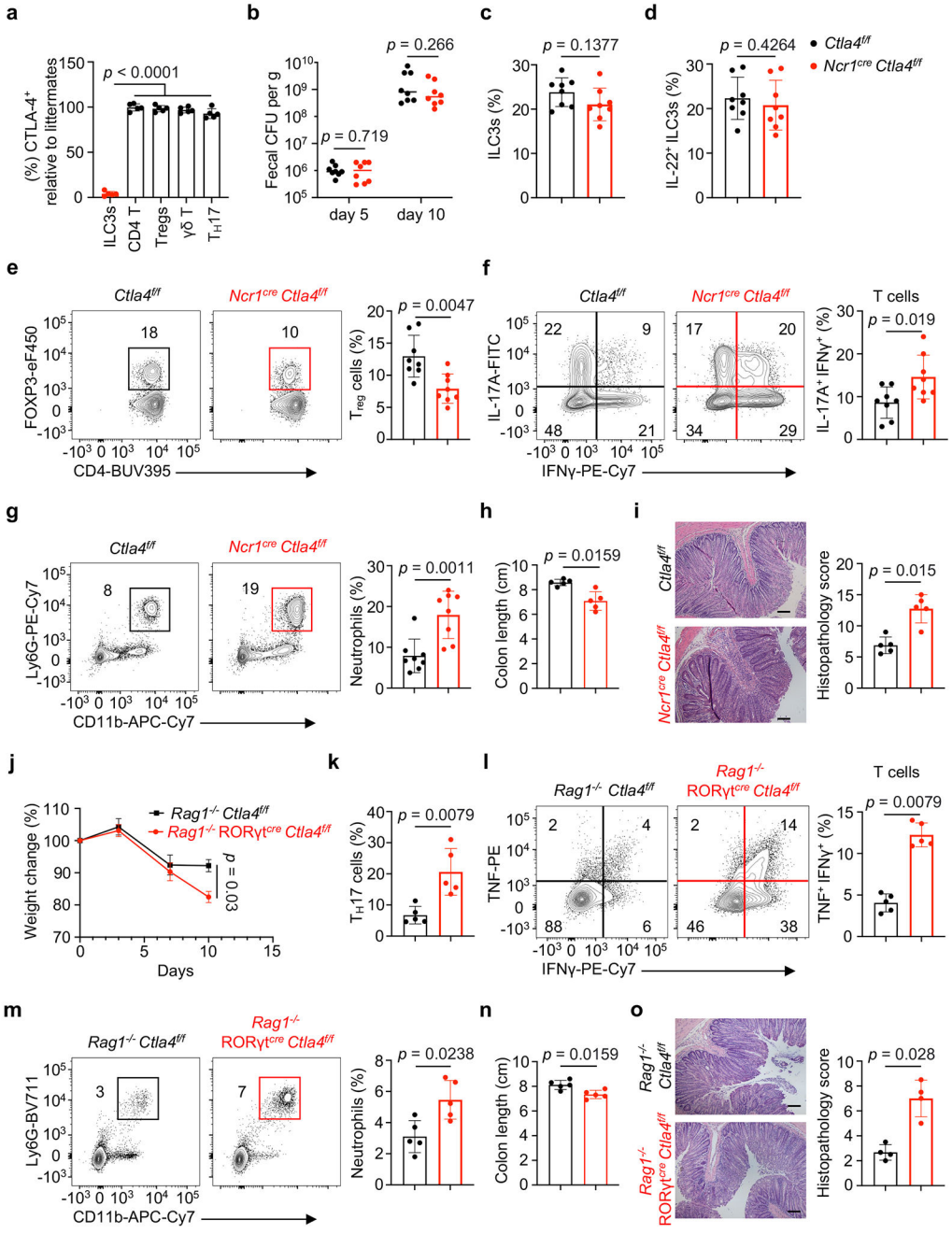

Figure 3 |. CTLA-4$^+$ ILC3s restrains IL-23-dependent gut inflammation.

a, Percentage of CTLA-4$^+$ immune cells (n = 5 mice). Mice were infected with *C. rodentium*, (**b**) fecal bacteria at indicated days post infection (dpi; n = 8 mice). Immune cells in large intestine at 14 dpi. Graph displaying frequency of (**c**) ILC3s (percentage of Lin$^-$CD90$^+$CD127$^+$ cells) and (**d**) IL-22$^+$ ILC3s (percentage of total ILC3s; n = 8 mice). **e,** Flow cytometry plots with graph of Treg frequency among CD4$^+$ T cells (n = 8 mice)**.** **f**, Flow cytometry plots with graph of IL-17A$^+$IFNγ^+ cell frequency among CD4$^+$ T cells (n = 8 mice). **g,** Flow cytometry plots with graph of neutrophil frequency among CD45$^+$

cells (n = 8 mice) with (**h**) colon lengths at 14 dpi (n = 5 mice). **i**, H&E staining and histopathology score of distal colon at 14 dpi (n = 5 mice). Scale bars, 50 μm. Naïve $CD4^+$ T cells were transferred to recipient mice and analyzed 11 days later. **j,** Graph of weight loss (n = 5 mice). Immune cells in large intestine and (**k**) graph of T_H17 cell frequency among $CD4^+$ T cells (n = 5 mice)**. l**, Flow cytometry plots with $TNF^+IFN\gamma^+$ cell frequency among $CD4^+$ T cells (n = 5 mice). **m,** Flow cytometry plots with graph of neutrophil frequency among $CD45^+$ cells (n = 5 mice) with (**n**) colon length (n = 5 mice). **o**, H&E staining and histopathology score of distal colon (n = 4 mice). Scale bars, 50 μm. Data in **a,h**, and **i** are representative of two independent experiments. Data in **b-g** and **j-o** were pooled from two independent experiments. All data shown as Mean ± s.d.. The statistics in **a** was calculated by one-way ANOVA with Dunnett's multiple comparisons and in **b-o** by Mann–Whitney U-test (unpaired, two-tailed).

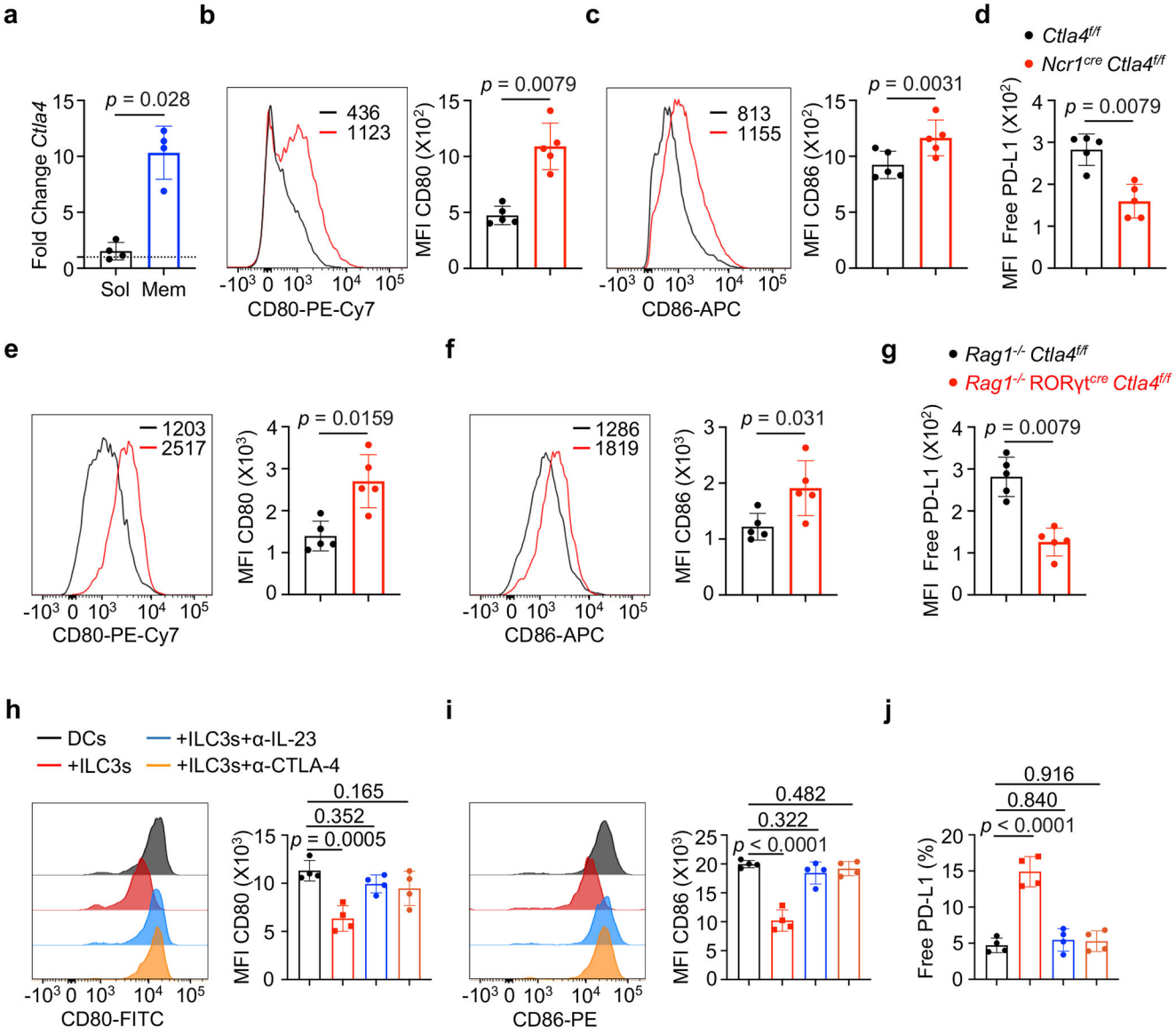

Figure 4 |. CTLA-4$^+$ ILC3s regulate co-stimulatory and inhibitory checkpoints on myeloid cells in the gut.

a, Relative soluble (Sol) and membrane (Mem) *Ctla4* transcripts in the sort-purified ILC3s stimulated with IL-23 ($n = 4$ mice). The dotted line represents fold change of 1. Mice were orally infected with *C. rodentium*, and myeloid cells in large intestine lamina propria were analyzed at 14 dpi. Flow cytometry plots with graph of MFI for (**b**) CD80 and (**c**) CD86 and (**d**) free-PD-L1 expression on myeloid cells gated as CD11c$^+$ MHCII^{hi} ($n = 5$ mice). Naïve CD4$^+$ T cells were adoptively transferred to recipient mice and myeloid cells in large intestine lamina propria were analyzed at day 11 post transfer. Flow cytometry plots with graph of MFI for (**e**) CD80 and (**f**) CD86 and (**g**) free-PD-L1 expression on myeloid cells gated as CD11c$^+$ MHCII^{hi} ($n = 5$ mice). Sorted ILC3s and myeloid cells from the large intestine lamina propria of C57BL/6 mice were co-cultured with heat killed *C. rodentium* for 20 hours in different conditions. Flow cytometry plots with graph of MFI for (**h**) CD80 and

(**i**) CD86 expression on myeloid cells gated as $CD11c^{+}$ $MHCII^{hi}$ ($n = 4$ mice). **j,** Graph of free PD-L1 frequency on myeloid cells gated as $CD11c^{+}$ $MHCII^{hi}$ ($n = 4$ mice). Data in **a-j** are representative of two or three independent experiments with similar results and shown as Mean ± s.d.. The statistics in **a-j** were obtained by Mann–Whitney *U*-test (unpaired, two-tailed).

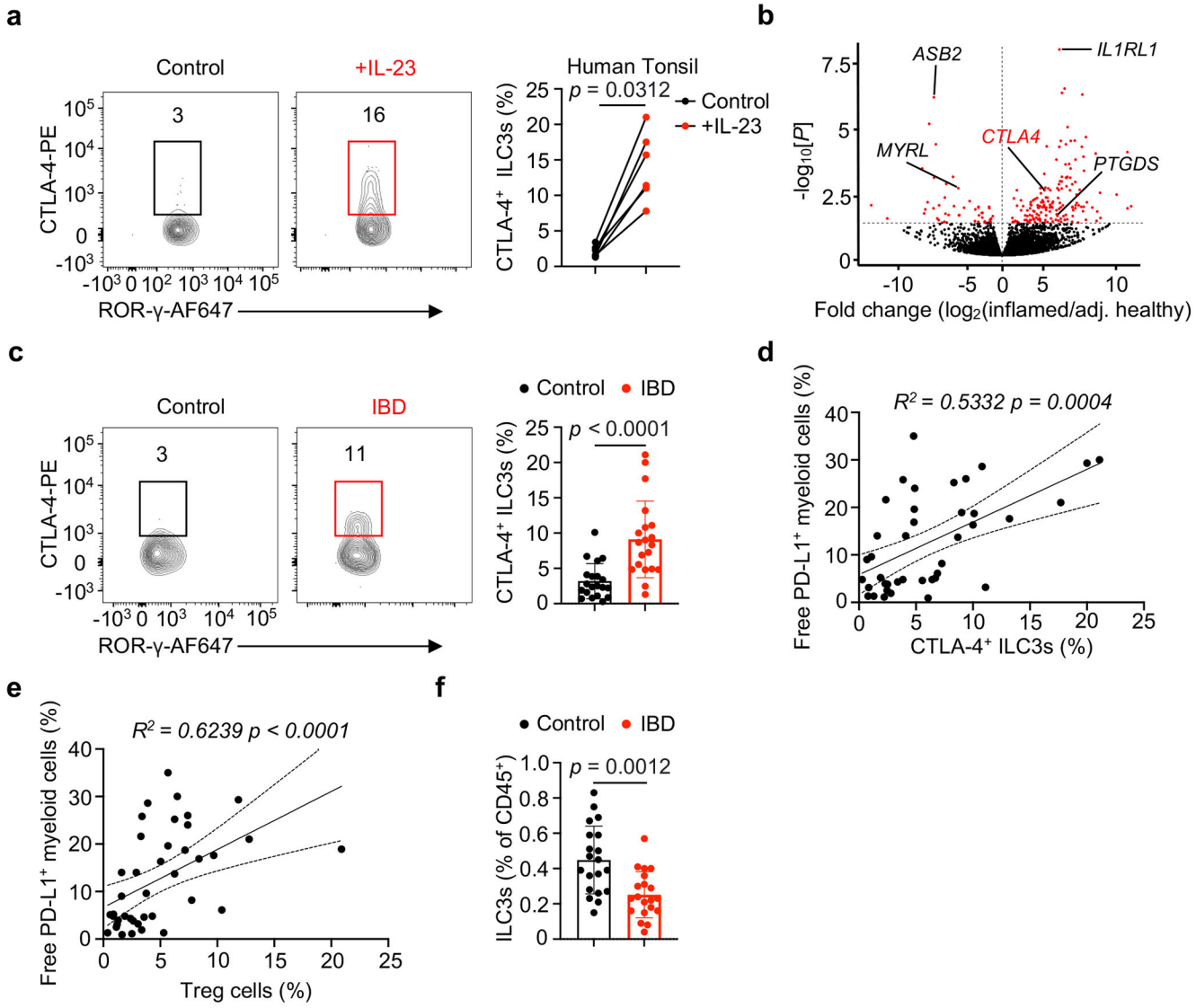

Figure 5 |. IL-23 upregulates CTLA-4$^+$ ILC3s in humans and this axis is altered in IBD.

a, Flow cytometry plots with graph of CTLA-4$^+$ ILC3 frequency (percentage of total ILC3s) from human tonsils stimulated for 6 hours with or without recombinant human IL-23 (n = 6 human samples). **b,** Volcano plot of differentially expressed genes (DEGs) in bulk RNA-seq dataset of ILC3s sorted from the inflamed or normal adjacent intestinal tissue of IBD patients**.** Immune cells were isolated from intestinal biopsies of 20 healthy human controls or patients with Crohn's disease (CD) and (**c**) flow cytometry plots with graph of CTLA-4$^+$ ILC3 frequency gated as CD45$^+$ Lin$^-$ CD127$^+$ RORγ^+ cells (percentage of total ILC3s). **d**, Frequency of CTLA-4$^+$ ILC3s (percentage of total ILC3s) were correlated with frequency of free PD-L1$^+$ myeloid cells (percentage of total myeloid cells) gated as CD45$^+$ CD11c$^+$ MHCII$^+$ cells (n = 20 non-IBD human controls; n = 20 human patients with CD). **e,** Frequency of free PD-L1$^+$ myeloid cells (percentage of total myeloid cells) were correlated with Tregs frequency gated as CD45$^+$ CD3$^+$ CD4$^+$ FOXP3$^+$ of CD4$^+$ T cells (n = 20 non-IBD human controls; n = 20 human patients with CD). **f,** Graph of

ILC3 frequency gated as $CD45^+$ Lin^- $CD127^+$ $ROR\gamma^+$ cells relative to total $CD45^+$ cells (n = 20 non-IBD human controls; n = 20 human patients with CD). The statistics in **a,** were calculated using Wilcoxon matched-pairs test (paired, two-tailed). The statistics in **b** were calculated using the Wald test within DESeq2. The statistics in **c** and **f** were calculated by Mann–Whitney *U*-test (unpaired, two-tailed). Correlative analyses in **d** and **e** were calculated by non-parametric Spearman correlation. Data in **a** are representative of two independent experiments, shown as mean ± s.d.